

1 **Short title:**

2 BCAA catabolism requires GRXS15 function

3

4

5

6 **Corresponding author:**

7 Andreas J. Meyer

8 Institute of Crop Science and Resource Conservation (INRES), Chemical Signalling, University

9 of Bonn

10 Friedrich-Ebert-Allee 144, D-53113 Bonn, Germany

11 Phone: +49 228 73 60353

12 Email: andreas.meyer@uni-bonn.de

13

14

15

16 **Research Area:**

17 Biochemistry and Metabolism

18

19 **Branched-chain amino acid catabolism depends on GRXS15 through**
20 **mitochondrial lipoyl cofactor homeostasis**

21

22 **Anna Moseler^{a,b}, Inga Kruse^{c,d}, Andrew E. Maclean^{c,d,*}, Luca Pedroletti^a, Stephan Wagner^a,**
23 **Regina Wehler^f, Katrin Fischer-Schrader^g, Gernot Poschet^h, Markus Wirtz^h, Peter**
24 **Dörmann^f, Tatjana M. Hildebrandtⁱ, Rüdiger Hell^h, Markus Schwarzländer^e, Janneke**
25 **Balk^{c,d}, Andreas J. Meyer^{a,j}**

26

27 ^aInstitute of Crop Science and Resource Conservation (INRES) - Chemical Signalling,
28 University of Bonn, 53113 Bonn, Germany

29 ^bUniversité de Lorraine, INRAE, IAM, 54000 Nancy, France

30 ^cJohn Innes Centre, NR4 7UH Norwich, UK

31 ^dUniversity of East Anglia, NR4 7TJ Norwich, UK

32 ^eInstitute of Plant Biology and Biotechnology (IBBP) – Plant Energy Biology, University of
33 Münster, 48143 Münster, Germany

34 ^fInstitute of Molecular Physiology and Biotechnology of Plants (IMBIO), University of Bonn,
35 53115 Bonn, Germany

36 ^gDepartment of Chemistry, Institute for Biochemistry, University of Cologne, 50674 Cologne,
37 Germany

38 ^hCentre for Organismal Studies, University of Heidelberg, 69120 Heidelberg, Germany

39 ⁱInstitute of Plant Genetics, Leibniz University Hannover, 30167 Hannover Germany

40 ^jBioeconomy Science Center, c/o Forschungszentrum Jülich, 52425 Jülich, Germany

41 *current address: Wellcome Centre for Integrative Parasitology, University of Glasgow, G12
42 8TA, Glasgow, UK

43

44

45 **One-sentence summary:**

46 Deficiency in GRXS15 restricts protein lipoylation and causes metabolic defects in lipoyl
47 cofactor-dependent dehydrogenase complexes, with branched-chain amino acid catabolism as
48 dominant bottleneck.

49

50

51 **Footnotes:**

52 **Author contributions**

53 A.M. and A.J.M. conceived the research with specific input from M.S. and J.B.; A.M. A.J.M. and
54 J.B. designed the experiments and interpreted the data. I.K., A.E.M., S.W., R.W., K.F.-S., G.P.,
55 M.W., T.M.H and L.P. contributed experimental data and structural information and analyzed the
56 data. A.M. and A.J.M. wrote the manuscript with support from M.S., T.H., M.W. R.H., P.D. and
57 J.B.; A.J.M. agrees to serve as the author responsible for contact and ensures communication.

58

59

60 **Funding Information**

61 This work was supported by grants of the German Research Foundation (Deutsche
62 Forschungsgemeinschaft, DFG) through the priority program SPP1710 'Dynamics of thiol-based
63 redox switches in cellular physiology' (ME1567/9-1/2, SCHW1719/7-1, HE1848/16-1), the
64 Emmy Noether programme (SCHW1719/1-1), an individual grant (ME1567/13-1), and through
65 the Research Training Group 2064 'Water use efficiency and drought stress responses: From
66 Arabidopsis to Barley'. A.M. is also recipient of a Feodor Lynen Research Fellowship from the
67 Alexander von Humboldt Foundation.

68

69

70 **Author for contact:**

71 Andreas.meyer@uni-bonn.de

72

73 **Abstract**

74 Iron-sulfur (Fe-S) clusters are ubiquitous cofactors in all life and are used in a wide array of
75 diverse biological processes, including electron transfer chains and several metabolic pathways.
76 Biosynthesis machineries for Fe-S clusters exist in plastids, the cytosol and mitochondria. A
77 single monothiol glutaredoxin (GRX) has been shown to be involved in Fe-S cluster assembly in
78 mitochondria of yeast and mammals. In plants, the role of the mitochondrial homologue
79 GRXS15 has only partially been characterized. Arabidopsis *grxs15* null mutants are not viable,
80 but mutants complemented with the variant *GRXS15 K83A* develop with a dwarf phenotype. In
81 an in-depth metabolic analysis, we show that most Fe-S cluster-dependent processes are not
82 affected, including biotin biosynthesis, molybdenum cofactor biosynthesis and the electron
83 transport chain. Instead, we observed an increase in most TCA cycle intermediates and amino
84 acids, especially pyruvate, 2-oxoglutarate, glycine and branched-chain amino acids (BCAAs).
85 The most pronounced accumulation occurred in branched-chain α -keto acids (BCKAs), the first
86 degradation products resulting from deamination of BCAAs. In wild-type plants, pyruvate, 2-
87 oxoglutarate, glycine and BCKAs are all metabolized through decarboxylation by four
88 mitochondrial lipoyl cofactor-dependent dehydrogenase complexes. Because these enzyme
89 complexes are very abundant and the biosynthesis of the lipoyl cofactor depends on continuous
90 Fe-S cluster supply to lipoyl synthase, this could explain why lipoyl cofactor-dependent
91 processes are most sensitive to restricted Fe-S supply in *GRXS15 K83A* mutants.

92

93

94 Introduction

95 Since the early days of biological evolution iron-sulfur (Fe-S) clusters have been
96 employed as catalytic co-factors for electron transfer reactions and are nowadays present in a
97 plethora of essential proteins (Pain and Dancis, 2016). Because Fe-S clusters are inherently
98 instable they do not exist in free form but always need to be chaperoned before reaching their
99 final destination apoproteins. Among the proteins thought to be involved in Fe-S cluster transfer
100 downstream of the assembly machinery is a specific subtype of glutaredoxins (GRXs) capable
101 of coordinating [2Fe-2S] clusters as a protein dimer (Banci et al., 2014; Couturier et al., 2015;
102 Lill and Freibert, 2020).

103 Glutaredoxins are ubiquitous proteins, which form a large family with several subfamilies
104 in plants (Rouhier et al., 2008; Meyer et al., 2009). Although their canonical function is
105 glutathione-dependent redox catalysis, dissection of the function of subclasses and individual
106 family members reveals an unexpectedly diverse picture (Lillig et al., 2008; Deponte, 2013).
107 Class II GRXs share a CGFS amino acid motif in the active site and are proposed to serve as
108 carrier proteins for Fe-S cluster between the assembly machinery and receiving apoproteins. A
109 second proposed function is the repair of oxidation sensitive Fe-S clusters (Couturier et al.,
110 2015). In Arabidopsis, Fe-S cluster assembly machineries are present in the cytosol, plastids
111 and mitochondria and at least one monothiol GRX is located in each of these compartments:
112 GRXS15 in mitochondria; GRXS14 and GRXS16 in plastids; and GRXS17 in the cytosol (Cheng
113 et al., 2006; Bandyopadhyay et al., 2008; Moseler et al., 2015; Knesting et al., 2015). While
114 autonomous pathways for the multistep Fe-S protein maturation process are present in plastids
115 and mitochondria, the cytosolic machinery relies on the export of bound sulfide as a precursor
116 from mitochondria (Schaedler et al., 2014). While plants deficient in plastidic GRXS14 did not
117 display any growth phenotype under non-stress conditions, genetic stacking of a *grxs14* null
118 mutant and knockdown of GRXS16 caused pronounced growth retardation (Rey et al., 2017).
119 Exposure of *grxs14* and the double mutant to prolonged darkness led to accelerated chlorophyll
120 loss compared to wild type (WT) and decreased abundance of proteins involved in the
121 maturation of Fe-S proteins. Mutants lacking the cytosolic GRXS17 were sensitive to high
122 temperature and long-day photoperiod (Cheng et al., 2011; Knesting et al., 2015). However,
123 the activities of cytosolic Fe-S proteins, like aconitase (ACO) or aldehyde oxidase, were not
124 substantially altered in *grxs17* null mutants (Knesting et al., 2015; Iñigo et al., 2016).

125 The mitochondrial GRXS15 is indispensable as indicated by embryonic lethality of null
126 mutants (Moseler et al., 2015). Partial complementation with a mutated *GRXS15 K83A* variant,
127 which is weakened in its ability to coordinate an [2Fe-2S] cluster *in vitro*, results in a dwarf
128 phenotype and diminished activity of the Fe-S protein ACO (Moseler et al., 2015). A similar
129 dwarf phenotype has also been reported for a GRXS15 knockdown line, albeit without any effect

130 on ACO activity (Ströher et al., 2016). Mitochondria contain at least 26 Fe-S proteins that are
131 involved in different processes, including electron transport (complexes I, II and III in the
132 respiratory electron transport chain) and the tricarboxylic acid (TCA) cycle [ACO and succinate
133 dehydrogenase (SDH)]. A general role of GRXS15 in the early steps of Fe-S cluster transfer
134 would therefore predict pleiotropic effects of diminished GRXS15 activity, due to the
135 simultaneous impairment of several central mitochondrial processes. The number of potential
136 defective sites is even further amplified if the synthesis of enzyme cofactors and the function of
137 several cofactor-dependent enzymes, in turn, is compromised. Indeed, pathways for
138 biosynthesis of the molybdenum cofactor (Moco) and lipoyl cofactor involve the mitochondrial
139 [4Fe-4S] proteins GTP-3',8-cyclase CNX2 (cofactor of nitrate reductase and xanthine
140 dehydrogenase 2) and LIP1 (lipoyl synthase) (Yasuno and Wada, 2002; Schwarz and Mendel,
141 2006).

142 A pronounced decrease in lipoyl cofactor-dependent proteins in GRXS15 knockdown
143 mutants led to the conclusion that efficient transfer of Fe-S clusters is required for mitochondrial
144 lipoyl cofactor synthesis (Ströher et al., 2016). In the mitochondrial matrix, four enzyme
145 complexes depend on lipoamide as a prosthetic group: the pyruvate dehydrogenase complex
146 (PDC), the 2-oxoglutarate dehydrogenase complex (OGDC), the glycine decarboxylase
147 complex (GDC), and the branched-chain α -keto acid dehydrogenase complex (BCKDC) (Taylor
148 et al., 2004; Solmonson and DeBerardinis, 2018). The PDC acts as the entry point of acetyl-
149 CoA into the TCA cycle, while OGDC acts within the TCA cycle to convert 2-oxoglutarate to
150 succinyl-CoA. The GDC catalyzing the oxidative decarboxylation of glycine is essential for
151 photorespiration (Douce et al., 2001), but also for C1 metabolism (Mouillon et al., 1999).
152 BCKDC is involved in catabolism of the three branched-chain amino acids (BCAAs) leucine
153 (Leu), valine (Val) and isoleucine (Ile) and their corresponding branched-chain α -keto acids
154 (BCKAs) (Gu et al., 2010; Araújo et al., 2010; Peng et al., 2015). Whether all these lipoyl
155 cofactor-dependent enzymes are affected similarly in *grxs15* mutants and whether other
156 pathways containing Fe-S enzymes are diminished and thus constitute bottlenecks that severely
157 restrict metabolic fluxes is yet unknown because the respective mutants have not been
158 metabolically characterized.

159 Here, we aimed to identify the most severe metabolic bottlenecks caused by severely
160 restricted capacity of GRXS15 mutants in Fe-S transfer. We consider several candidate Fe-S
161 proteins involved in essential mitochondrial processes starting with biotin biosynthesis, followed
162 by Moco biosynthesis, capacity of the mitochondrial electron transport chain, TCA cycle flow
163 and closing with the biosynthesis of lipoyl cofactor. We assess how these Fe-S related
164 processes are affected in *grxs15-3* null mutants complemented with *GRXS15 K83A* and in
165 *GRXS15^{amiR}* knockdown mutants trying to pin down the cause of the phenotype and by that the

166 functional significance of GRXS15. By direct comparison of partially complemented null mutants
167 and knockdown mutants we resolve previous contradictions about the role of GRXS15 in the
168 maturation of Fe-S containing enzymes.

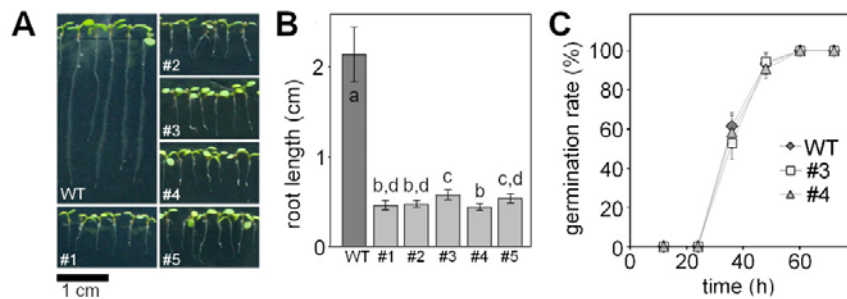
169

170

171 **Results**

172 ***GRXS15 K83A* causes retardation in growth**

173 To complete embryogenesis, *GRXS15* is essential in plants. To bypass embryo lethality,
174 *Arabidopsis grxs15* null mutants were complemented with the *GRXS15 K83A* variant which are
175 able to grow, but the plants have small rosette leaves (Moseler et al., 2015). Based on that
176 observation we aimed to further analyze the growth phenotype and compare with published
177 records of *grxs15* knockdown mutants. A dwarf phenotype of the *GRXS15 K83A*
178 complementation lines #1 to #5 becomes apparent at the early seedling stage (Fig. 1A, B).
179 Analysis of root length in five randomly selected lines consistently also showed a concomitant
180 reduction of primary root length compared to WT (Figure 1B).
181



182

183 **Figure 1. Complementation of the *Arabidopsis grxs15-3* mutant with *UBQ10_{pro}:GRXS15 K83A*.**

184 **A:** 8-d-old wild-type (WT) seedlings compared with *GRXS15 K83A* mutants grown on vertical agar plates
185 under long-day conditions.

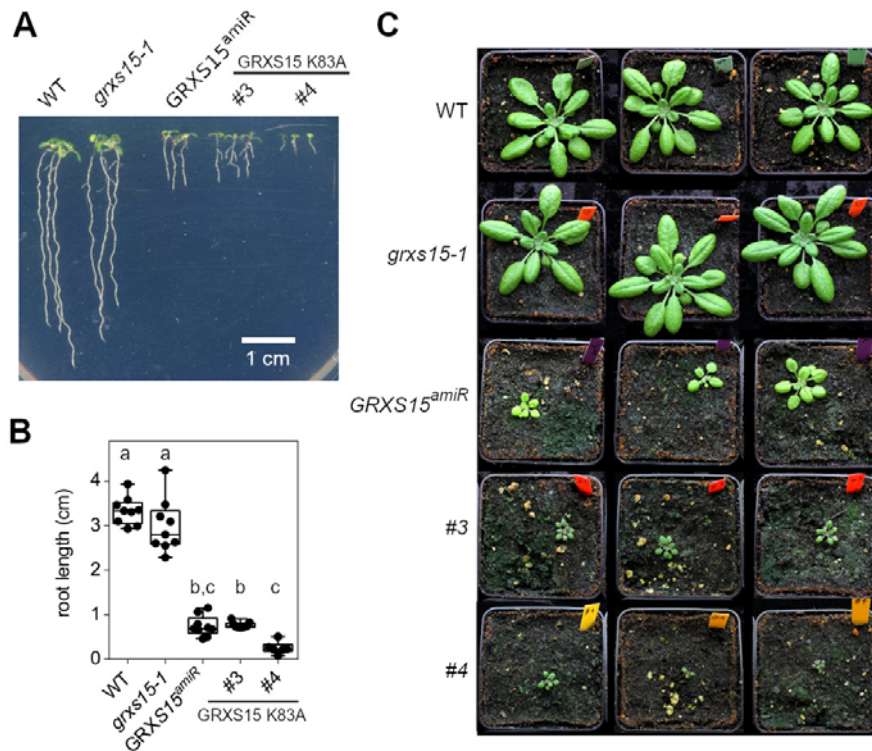
186 **B:** Primary root length of 8-d-old *GRXS15 K83A* mutants compared to WT ($n = 35$; means \pm SD).
187 Different letters indicate significant differences between the different lines; $P \leq 0.05$; (one-way ANOVA
188 with post hoc Holm-Sidak).

189 **C:** Germination rate of *GRXS15 K83A* lines #3 and #4 compared to WT. All seeds were initially stratified
190 at 4°C in the dark for 1 d ($n = 6$ with 20-25 seeds each; means \pm SD). Germination was assessed with the
191 emergence of the radicle. No statistically significant differences were found using Student's t-Test
192 analysis.

193

194 Although only minor differences in seedling size could be observed, line #3 was the best
195 growing complementation line and line #4 the weakest (Fig.1C; Moseler et al., 2015). This effect
196 was stable and consistent over several generations. The phenotype is similar to *GRXS15amiR*
197 knockdown lines reported by Ströher et al. (2016) (Supplemental Fig. S1). A T-DNA insertion
198 line *grxs15-1* carrying a T-DNA in an intron within the 5'-UTR (Moseler et al., 2015), which had
199 been reported to display a short root phenotype (Ströher et al., 2016) cannot be clearly
200 distinguished from the WT in our hands, neither at seedling stage nor at rosette stage
201 (Supplemental Fig. S1). This allele was excluded from further analysis. To test whether the
202 reduced growth of *GRXS15 K83A*-complemented null mutants was true growth retardation or
203 caused by delayed germination, the two lines #3 and #4 were scored for the timing of radical

204 emergence. The absence of any difference between WT and the two mutants suggests that the
205 growth phenotype reflects a genuine growth retardation (Fig. 1C).
206



207

208 **Supplemental Figure S1: Arabidopsis mutants affected in GRXS15 function develop a dwarf**
209 **phenotype.**

210 **A, B:** Growth of different *grxs15* mutants (*grxs15-1*, *GRXS15^{amiR}*, *GRXS15 K83A* lines #3 and #4) and
211 wild-type (WT) seedlings on vertical plates with 0.8% agar under long-day conditions. Seedlings were
212 documented and quantitatively analyzed for their root length 10 days after germination. ($n = 6-9$; box plot
213 shows means with whiskers indicating min and max values). Different letters indicate significant
214 differences between the different lines; $P \leq 0.05$; (one-way ANOVA).

215 **C:** Phenotypes of soil-grown plants after five weeks under long-day conditions (16 h light, 19°C, 8 h dark,
216 17°C; 50% rh).
217

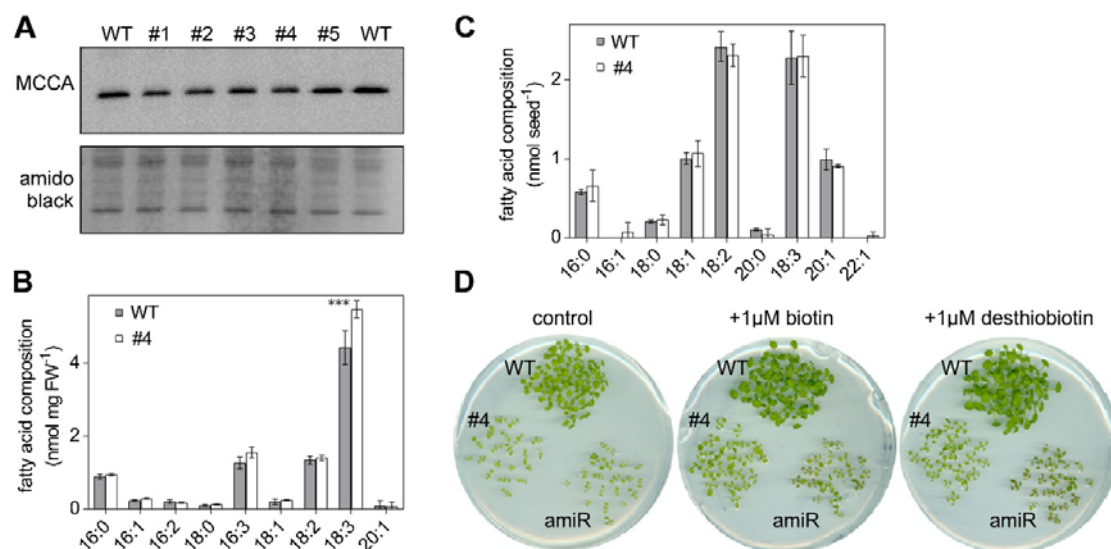
218

219 **Biotin-mediated metabolism is not impaired when GRXS15 function is diminished**

220 Following our earlier observation that GRXS15 can coordinate a [2Fe-2S] cluster
221 (Moseler et al., 2015), similar to the closest homologs in yeast and mammals (Uzarska et al.,
222 2013; Banci et al., 2014), we embarked on testing a number of pathways of Fe-S-dependent
223 metabolism that may be affected in the mutant. One putative target protein of GRXS15 is
224 mitochondrial biotin synthase (BIO2, At2g43360) since it relies on supply of a [2Fe-2S] and a
225 [4Fe-4S] cluster. BIO2 catalyzes the final step in biotin biosynthesis, which acts as an essential
226 cofactor in several carboxylases in energy metabolism. Destruction of the [2Fe-2S] cluster for
227 sulfur supply to biotin with each catalytic cycle and subsequent turnover increases the demand
228 for [2Fe-2S] clusters (Ugulava et al., 2001). *bio2* null mutants were previously described as
229 embryo-defective, arrested mostly at globular or heart stage of embryo development (Patton et
230 al., 1998; Meinke, 2019). Because lack of biotin typically causes degradation of the respective
231 apoproteins (Solbiati et al., 2002), we tested for the abundance of biotin-dependent
232 methylcrotonoyl-CoA carboxylase (MCCase), which is involved in leucine degradation in
233 mitochondria. None of the five analyzed *grxs15* complementation lines showed a decrease in
234 protein abundance of the biotinylated MCCase subunit A (MCCA) (Fig. 2A). Biotin is also
235 exported to the cytosol and the chloroplasts, where it is required for synthesis and elongation of
236 fatty acids by hetero- and homomeric acetyl-CoA carboxylase (ACCase). Total fatty acids in
237 seeds amounted to 7.6 ± 0.8 nmol seed⁻¹ in line #4 and 7.6 ± 1.0 nmol seed⁻¹ in the WT and no
238 difference in relative abundance of specific fatty acids in seeds was observed (Fig. 2C). In 8-
239 day-old seedlings the amount of total fatty acids did not differ in line #4 10.3 ± 0.4 nmol (mg
240 FW)⁻¹ compared to 8.8 ± 1.0 nmol (mg FW)⁻¹ in WT, but a 23% increase in α -linolenic acid (18:3)
241 was observed (Fig. 2B).

242 *bio2* mutants can be rescued by the addition of biotin to both arrested embryos cultured
243 *in vitro* and to mutant plants grown on soil (Schneider et al., 1989; Patton et al., 1998;
244 Pommerrenig et al., 2013). External supply of biotin or its precursor desthiobiotin to a
245 *GRXS15*^{amiR} knockdown mutant and the complemented line #4 in both cases improved growth
246 slightly but did not rescue the growth defects of either of the lines (Fig. 2D). It should be noted
247 though that also the WT grew better with supply of biotin or desthiobiotin. These results suggest
248 that growth retardation of *grxs15* mutants is not primarily caused by defects in biotin synthesis.

249



250

251 **Figure 2. *GRXS15 K83A* mutation has no impact on the biotin pathway in *Arabidopsis* seedlings.**

252 **A:** Immunoblot analysis of biotinylated MCCA in mitochondria of *GRXS15 K83A* mutants compared with
 253 WT. In the upper panel, biotinylated MCCA was detected by streptavidin HRP in isolated mitochondria
 254 from 2-weeks-old seedlings (9 μg protein was loaded per lane). In the lower panel, amido black staining
 255 of the membrane is shown as a control for protein loading.

256 **B, C:** Fatty acids quantified by gas chromatography using a flame ionization detector of 8-d-old seedlings
 257 (B) and seeds (C) of *GRXS15 K83A* line #4 compared to WT ($n = 3-4$; means \pm SD). The statistical
 258 analysis (two-way ANOVA with post hoc Holm-Sidak comparisons for WT vs. *grxs15*) indicated no
 259 significant ($P \leq 0.05$) change except for 18:3 (*** = $P < 0.001$).

260 **D:** *GRXS15 K83A* line #4, the knockdown line *GRXS15^{amiR}* (amiR) and wild-type plants were grown on
 261 horizontal plates with 1/2 MS agar without sucrose. The medium contained either no biotin (control), 1 μM
 262 biotin or 1 μM desthiobiotin.
 263

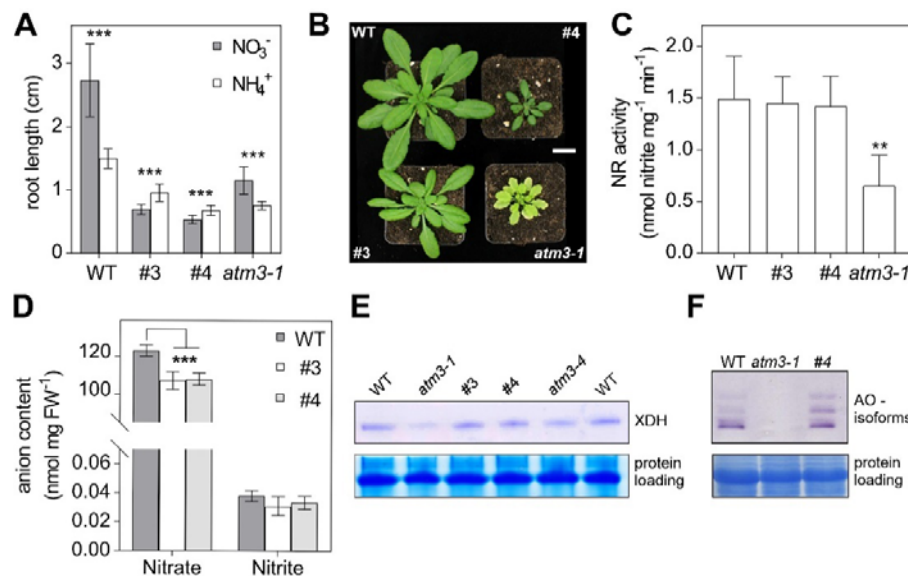
264

265 Moco-dependent nitrogen metabolism is not limiting upon impaired *GRXS15* function

266 The Moco precursor cyclic pyranopterin monophosphate (cPMP) is synthesized in the
 267 mitochondrial matrix by CNX2 (At2g31955) and the cyclic pyranopterin monophosphate
 268 synthase CNX3 (At1g01290) and is exported to the cytosol for subsequent biosynthesis steps
 269 (Bittner, 2014; Kruse et al., 2018). Because CNX2 contains two [4Fe-4S] clusters, we
 270 hypothesized that Moco biosynthesis and hence Moco-dependent biochemical pathways may
 271 be affected by defects in mitochondrial Fe-S transfer. The most abundant Moco-dependent
 272 enzymes include nitrate reductase (NR), aldehyde oxidase (AO), xanthine dehydrogenase
 273 (XDH) and sulfite oxidase (SO). *Arabidopsis* generally prefers nitrate as nitrogen source
 274 (Sarasketa et al., 2014), but mutants deficient in Moco biosynthesis can be rescued by providing
 275 ammonium as a nitrogen source to bypass nitrate reductase (Wang et al., 2004; Kruse et al.,
 276 2018), revealing NR as the main recipient of Moco. While the preference for nitrate (KNO₃) over
 277 ammonium ((NH₄)₂SO₄) could be confirmed in wild-type plants, we found that the growth

278 retardation of *GRXS15 K83A* roots is more pronounced on nitrate than on ammonium as sole
 279 nitrogen source (Fig. 3A). Similar results were obtained when seedlings were grown on NH_4Cl
 280 instead of $(\text{NH}_4)_2\text{SO}_4$ to control for possible impacts of the respective counter anions on the
 281 growth behavior (Supplemental Fig. S2A).

282
 283



284

285 **Figure 3. Growth of Arabidopsis *GRXS15 K83A* mutants is affected by the nitrogen source.**

286 **A:** Primary root length of *GRXS15 K83A* lines #3 and #4 as well as *atm3-1* seedlings compared to WT
 287 grown on vertical agar plates containing 5 mM KNO_3 or 2.5 mM $(\text{NH}_4)_2\text{SO}_4$ as N-source for 8 d under
 288 long-day conditions ($n = 30$; means \pm SD). Student's t-Test analysis showed significant differences
 289 between the growth on the different inorganic N-sources in all lines ***: $P < 0.001$.

290 **B:** Representative 4-week-old plants of WT, *GRXS15 K83A* lines #3 and #4 and *atm3-1* all grown on soil
 291 under long-day conditions. Scale bar = 2 cm.

292 **C:** Nitrate reductase activity in WT, lines #3 and #4 as well as in *atm3-1*. Activity was analyzed in 4-week-
 293 old plants grown on soil by measuring the presence of nitrite via the Griess reaction ($n = 4$; means \pm SD,
 294 **: $P \leq 0.01$).

295 **D:** Nitrate and nitrite content of 8-d-old WT and *GRXS15 K83A* lines #3 and #4 seedlings grown on agar
 296 plates ($n = 4$; means \pm SEM). The statistical analysis (two-way ANOVA with post hoc Holm-Sidak
 297 comparisons for WT vs. *grxs15*) indicated a significant change in the nitrate content; ***: $P \leq 0.001$.

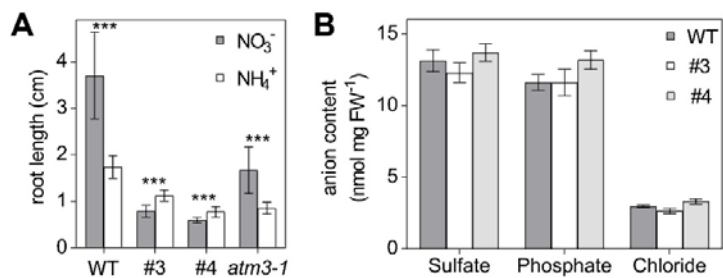
298 **E:** In-gel activity of XDH in WT, *atm3-1*, and *GRXS15 K83A* mutants. Equal amounts of protein (35 μg)
 299 extracted from 8-d-old seedlings were separated on non-denaturing PA gel and stained for XDH activity
 300 using hypoxanthine as substrate.

301 **F:** In-gel activities of aldehyde oxidase (AO) in WT and *atm3-1* as well as *grxs15* mutants. Equal amounts
 302 of protein were separated on non-denaturing PA gels and stained for AO activity using synthetic
 303 aldehydes (1-naphthaldehyde and indole-3-carboxaldehyde) as substrates. For control of protein-loading
 304 the gel was subsequently stained with Coomassie.

305
 306
 307

308 The pronounced growth retardation on nitrate could be indicative of severe NR
309 deficiency similar to *nia1 nia2* mutants lacking functional NR (Wilkinson and Crawford, 1993). A
310 similar NR deficiency has been described for mutant alleles of the ABC transporter ATM3 that is
311 involved in Moco biosynthesis (Bernard et al., 2009; Teschner et al., 2010; Kruse et al., 2018).
312 *atm3-1* mutants display a severe growth phenotype and are chlorotic (Fig. 3B). While *GRXS15*
313 *K83A* mutants are also smaller than WT, they are not chlorotic and thus do not phenocopy
314 *atm3-1* (Fig. 3A, B). Despite NR activity being diminished to 50% of WT, root growth of *atm3-1*
315 was still better on nitrate than on ammonium (Fig. 3A, C). NR activity was not altered in the
316 *GRXS15 K83A* mutants #3 and #4 (Fig. 3C). Despite the unaffected NR activity, both *grxs15*
317 mutants contained significantly less nitrate than WT seedlings (Fig. 3F). Nitrite and other
318 inorganic anions like chloride, sulfate or phosphate were not altered between the mutant lines
319 and WT (Supplemental Fig. S2B). All other tested Moco-dependent enzymes such as AO or
320 XDH showed no decrease in activity in the *grxs15* mutants compared to WT (Fig. 3E, F). Taken
321 together, these results suggest that NR activity in *GRXS15 K83A* mutants is sufficient to use
322 nitrate as the sole nitrogen source and does not explain the growth inhibition on nitrate.

323



324

325 **Supplemental Figure S2. Moco enzymes and anions are not affected in Arabidopsis *GRXS15 K83A***
326 **mutants**

327 **A:** Primary root length of *GRXS15 K83A* lines #3 and #4 as well as *atm3-1* mutant seedlings compared to
328 WT grown on vertical plates containing 5 mM KNO₃ or 5 mM NH₄Cl as N-source. Seedlings were grown
329 for 9 d under long-day conditions (*n* = 35; means ± SD). Student's t-Test analysis showed significant
330 differences between nitrate and ammonium treatment for each genotype (***: *P* ≤ 0.001).

331 **B:** Amount of sulfate, phosphate and chloride in Arabidopsis WT and line #3 and #4 seedlings (*n* = 4;
332 means ± SEM). The statistical analysis (two-way ANOVA with post hoc Holm-Sidak comparisons for WT
333 vs. *grxs15*) indicated no significant (*P* ≤ 0.05) change.

334

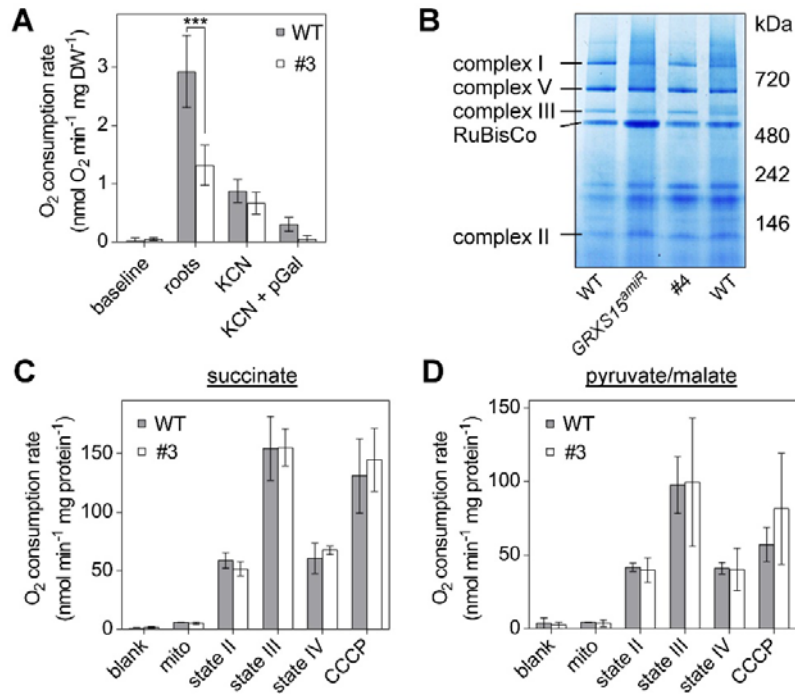
335

336

337 **Impaired GRXS15 function leads to decreased root respiration**

338 The mitochondrial *electron* transport chain (mETC) contains three enzyme complexes
339 with a total of 12 Fe-S cofactors: complex I with two [2Fe-2S] and six [4Fe-4S] clusters, complex
340 II with one [2Fe-2S], one [3Fe-4S], and one [4Fe-4S] cluster, and complex III with one [2Fe-2S]
341 cluster (Couturier et al., 2015; Meyer et al., 2019). Thus, we measured the respiration of
342 detached roots and dissected the capacity of complex I and II-linked electron flow. Indeed, roots
343 of line #3 displayed a decreased respiration rate of 1.31 ± 0.35 nmol O₂ min⁻¹ (mg DW)⁻¹
344 compared with the wild-type rate of 2.92 ± 0.62 nmol O₂ min⁻¹ (mg DW)⁻¹ (Fig. 4A). This is
345 similar to root tips of *GRXS15^{amiR}* knockdown plants which were reported to consume less
346 oxygen than wild-type plants (Ströher et al., 2016). Addition of the cytochrome c oxidase
347 inhibitor KCN decreased the rate of both lines down to similar values. The remaining rates are
348 accounted for by the presence of alternative oxidases (AOXs), since they could be inhibited by
349 propylgallate (pGal). Interestingly, the AOX capacity appeared unchanged in line #3, even
350 though AOX is highly inducible by mitochondrial dysfunction. Next, we investigated if the
351 decreased root respiration is due to defects in the respiratory machinery or due to restricted
352 metabolite turnover, or both. First, we compared the abundance of respiratory complexes in
353 isolated mitochondria from *GRXS15 K83A* line #4, *GRXS15^{amiR}* by BN-PAGE. None of the
354 respiratory complexes including the Fe-S cluster containing complexes I, II and III was
355 decreased in abundance in either mutant (Fig. 4B). Additionally, we purified mitochondria from
356 whole seedlings of the *GRXS15 K83A* line #3 and supplemented them with succinate or
357 pyruvate/malate, respectively, as respiratory substrates. Succinate provides electrons to the
358 ubiquinone pool of the mETC via complex II, whereas pyruvate/malate predominantly provides
359 NAD(P)H mainly generated by malate dehydrogenase and the PDC. NADH is subsequently
360 oxidized mainly by complex I of the mETC and NAD(P)H by matrix-exposed alternative NADH-
361 dehydrogenases. No differences in the respiration of isolated mitochondria were found with
362 supply of succinate or pyruvate/malate (Fig. 4C, D), suggesting that the differences in
363 respiration observed in whole roots cannot be accounted for by decreased capacities of the Fe-
364 S cluster-containing complexes. In summary, similar total respiratory activities of WT and
365 mutants further indicate that the *in vivo* difference in respiration rate is not due to a defect at the
366 level of the mETC, but rather upstream or downstream.

367



368

369 **Figure 4. Respiration in complemented Arabidopsis *grxs15* mutants.**

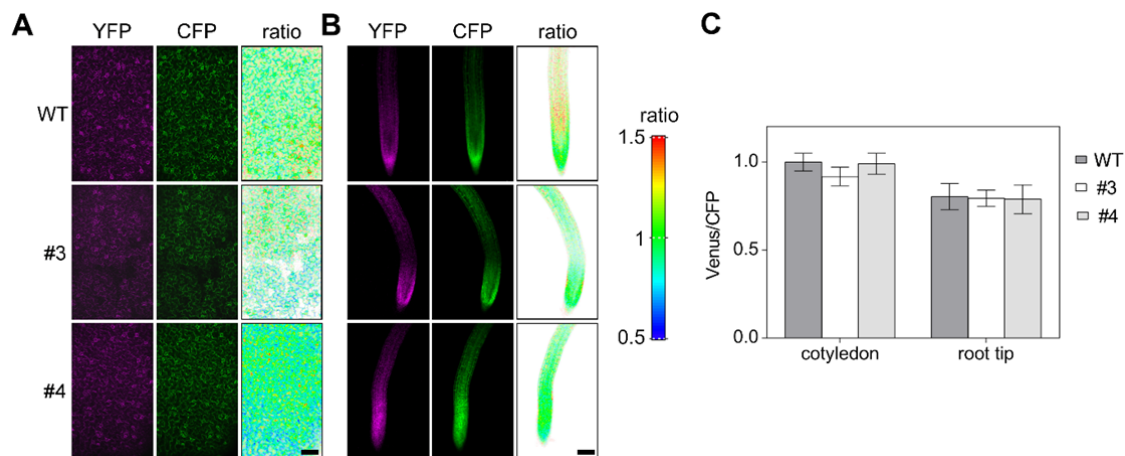
370 **A:** Root respiration rate of *GRXS15 K83A* line #3 (4.5-week-old) and the respective WT grown to similar
 371 size (2-week-old) after addition of the cytochrome c oxidase inhibitor KCN (4 mM) alone or together with
 372 the alternative oxidase inhibitor propylgallate (pGal; 0.2 mM) ($n = 4$; means \pm SD). The statistical analysis
 373 (two-way ANOVA with post hoc Holm-Sidak comparisons for WT vs. *grxs15* mutant) indicated a
 374 significant difference in the respiration of mitochondria from WT and *GRXS15 K83A* line #3; ***:
 375 $P \leq 0.001$.

376 **B:** Respiratory complexes I, II, III and V separated by BN-PAGE and visualized with Coomassie staining
 377 in WT, *GRXS15 K83A* line #4 and *GRXS15^{amiR}*. Mitochondria were purified from 4-week-old plants.

378 **C, D:** Oxygen consumption rates for purified mitochondria from WT and *GRXS15 K83A* line #3 energized
 379 with succinate or pyruvate/malate. O_2 consumption was measured before (blank) and after addition of
 380 mitochondria (mito). State II respiration was initiated by the addition of the respective substrate (state II;
 381 succinate (10 mM succinate, 0.25 mM ATP) or pyruvate/malate (10 mM pyruvate, 10 mM malate, 0.3 mM
 382 NAD and 0.1 mM thiamine pyrophosphate). State III respiration was initiated by the addition of 50 μ M
 383 ADP. State IV represents the respiration after ADP consumption and CCCP shows the respiration after
 384 addition of the protonophore carbonyl cyanide *m*-chlorophenylhydrazone (CCCP; 10 μ M), which
 385 uncouples electron transport from ATP synthesis. All results are based on three independent preparations
 386 of mitochondria and are shown as means \pm SEM.
 387

388 The *capacity* for electron flow in isolated mitochondria does not allow conclusions about
 389 the actual mETC *activity in planta*. Hence, we tested whether the decreased respiration rate
 390 may result in a change of the ATP status of the cells. For analyses of the $MgATP^{2-}$ level wild-
 391 type plants as well as the *grxs15* mutants #3 and #4 were transformed with the $MgATP^{2-}$
 392 biosensor ATeam1.03-nD/nA (De Col et al., 2017) targeted to the cytosol. As cytosolic ATP is
 393 predominantly provided by the mitochondria (Igamberdiev et al., 2001; Voon et al., 2018), any
 394 disturbance in the mitochondrial ATP synthesis will also affect the ATP level in the cytosol.
 395 Similar to the report by De Col et al. (2017) higher Venus/CFP fluorescence ratios indicating

396 more efficient FRET between the sensor subunits and hence higher $MgATP^{2-}$ levels were found
397 in cotyledons compared to roots (Supplemental Fig. S3). However, no differences in the
398 Venus/CFP emission ratio could be observed between WT and *GRXS15 K83A* mutants
399 indicating similar cytosolic ATP levels (Supplemental Fig. S3). It should be noted though that the
400 energy charge of the adenylate pool cannot be deduced from these results as it would require
401 also analysis of AMP and ADP.



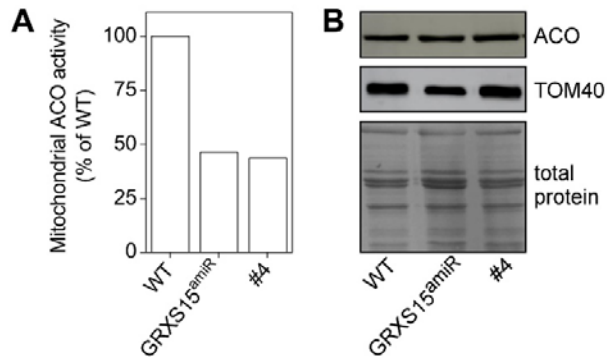
402

403 **Supplemental Figure S3. *In vivo* monitoring of ATP levels in the cytosol of Arabidopsis *GRXS15***
404 ***K83A* mutants.**

405 ATeam1.03-nD/nA was stably expressed under a 35S promoter in the cytosol of WT and *GRXS15 K83A*
406 lines #3 and #4 and analyzed in cotyledons (A) and roots (B) for fluorescence intensities of Venus and
407 CFP. Bars, 100 μ m. (C) Venus/CFP fluorescence ratios calculated from fluorescence images of
408 cotyledons and root tips of 7-d-old seedlings from two independent reporter lines for each genetic
409 background ($n = 10$; means \pm SD).

410

411 Previously we reported a 60% decrease in aconitase activity (Moseler et al., 2015),
412 which at last partially explain the decreased respiration rate, but a decrease in aconitase was
413 not seen in Ströher *et al.*, 2016. To clarify the situation, we measured the activity of ACO, a
414 [4Fe-4S] enzyme, in the *K83A* and *amiRNA* mutants grown under the same conditions side by
415 side. Despite similar amounts of ACO protein in mitochondria of WT and the mutants
416 *GRXS15^{amiR}* and *GRXS15 K83A #4*, ACO activity was decreased to approximately 40% in
417 isolated mitochondria of both mutants (Fig. 5). The observation that ACO activity is decreased,
418 while the ACO protein abundance is the same, is surprising because it is generally assumed
419 that ACO apoproteins are rather unstable and would be degraded (Castro et al., 2019). Either,
420 the ACO protein is stabilized in a yet unknown manner or ACO activity is compromised in
421 another way.



422

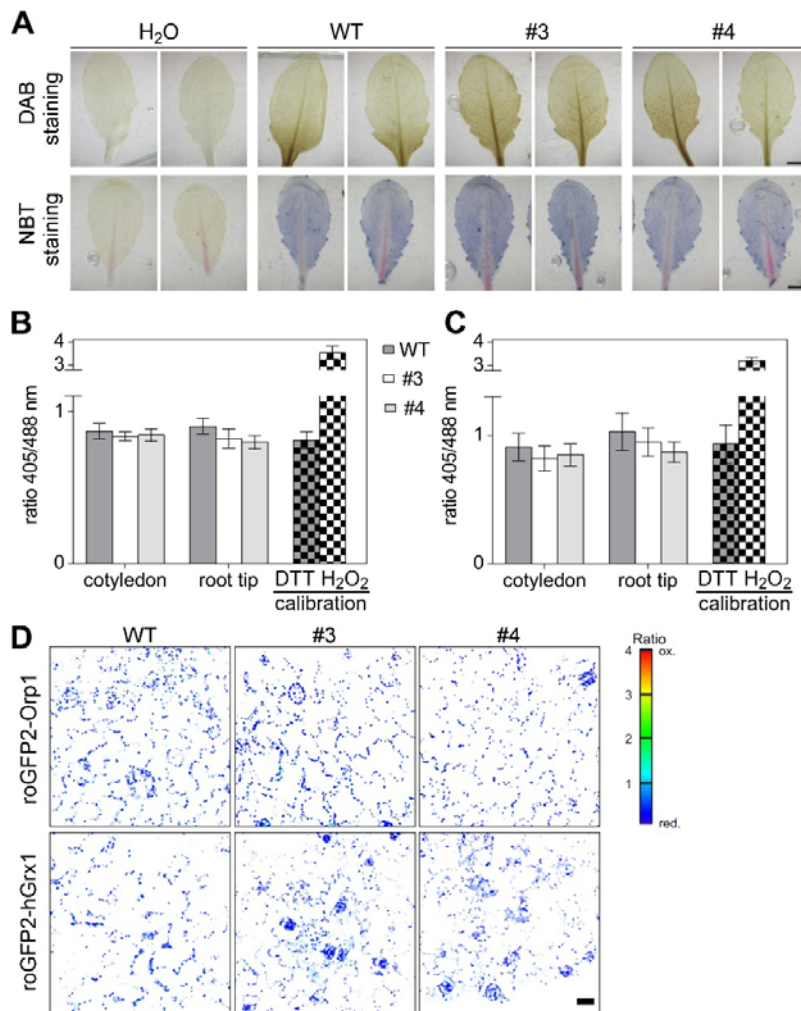
423 **Figure 5 Aconitase activities in mitochondria of *grxs15* mutants.**

424 **A:** Aconitase activity of *GRXS15^{amiR}* and *GRXS15 K83A* line #4 compared to the respective WT from
425 isolated mitochondria. $n = 2$.

426 **B:** Protein gel blot analysis probed with antiserum raised against Arabidopsis ACO. 9 μ g of protein
427 isolated from mitochondria of a wild-type plant as well as *GRXS15^{amiR}* and *GRXS15 K83A* lines #4 were
428 loaded onto the gel. ACO and translocase of the mitochondria 40 (TOM40) protein levels were visualized
429 by immunoblotting under denaturing conditions. Total protein staining served as a loading control.
430

431 **Diminished *GRXS15* activity does not lead to any major signs of oxidative stress**

432 Yeast Δ *grx5* mutant as well as a Arabidopsis *grxs14* null mutant are sensitive to
433 oxidative stress and at least for the Δ *grx5* it was shown that specific proteins are oxidized in this
434 mutant (Rodríguez-Manzaneque et al., 1999; Cheng et al., 2006). Aconitase is highly sensitive
435 to oxidative stress and redox metabolism in the matrix (Verniquet et al., 1991; Navarre et al.,
436 2000; Castro et al., 2019; Nietzel et al., 2020), suggesting that lower ACO activities may result
437 from iron-mediated ROS formation as a possible consequence of an improper Fe-S cluster
438 transfer by the *GRXS15 K83A* variant. However, staining of leaves with DAB for H₂O₂ and NBT
439 for superoxide revealed no differences between WT and *grxs15* mutants (Supplemental Fig.
440 S4). Since histological stains only provide a crude indication of major changes in ROS
441 dynamics, but are not sufficiently sensitive to resolve localized intracellular changes in oxidant
442 load, we next analyzed mitochondria-specific changes in H₂O₂ concentration or the glutathione
443 redox potential (E_{GSH}). The genetically encoded sensors roGFP2-Orp1 (Nietzel et al., 2019) and
444 roGFP2-hGrx1 (Albrecht et al., 2014) were expressed in the mitochondrial matrix of both WT
445 and mutant plants. Both sensors were highly reduced under control conditions and neither
446 roGFP2-Orp1 nor roGFP2-hGrx1 revealed any significant differences between WT and
447 *GRXS15 K83A* mutants in mitochondria of cotyledons and root tips (Supplemental Fig. S4B, C).
448 Both roGFP2-sensor variants remained highly reduced in all lines as indicated by similar
449 fluorescence ratios that resembled those after incubation with DTT for full sensor reduction. This
450 indicates no major oxidative challenge in the mitochondrial matrix. Both sensors were
451 responsive to oxidative challenge as indicated by a pronounced ratio change upon H₂O₂
452 addition.



453

454 **Supplemental Figure S4. Analysis of the oxidation state of the Arabidopsis *grxs15* mutants.**

455 **A:** Representative images showing DAB (upper) and NBT (lower) staining for detection of increased ROS
 456 production in leaves. Wild-type plants and mutants were grown for four weeks under long-day growth
 457 conditions. Bars, 0.5 cm. $n = 7-8$.

458 **B:** Ratiometric analysis of the H₂O₂-sensitive fluorescent reporter roGFP2-Orp1. 7-d-old seedlings of WT
 459 and *GRXS15 K83A* lines #3 and #4 expressing mitochondrial roGFP2-Orp1 were analyzed for the redox
 460 state of the sensor in cotyledons and root tips. For estimation of the dynamic range of the sensor, wild-
 461 type seedlings were incubated in 10 mM DTT (grey squared) or 10 mM H₂O₂ (white squared) and
 462 fluorescence of roGFP2 in the hypocotyl was analyzed. Ratios were calculated from fluorescence images
 463 of cotyledons and root tips of 7-d-old seedlings from two independent reporter lines for each genetic
 464 background ($n = 10$; means \pm SD).

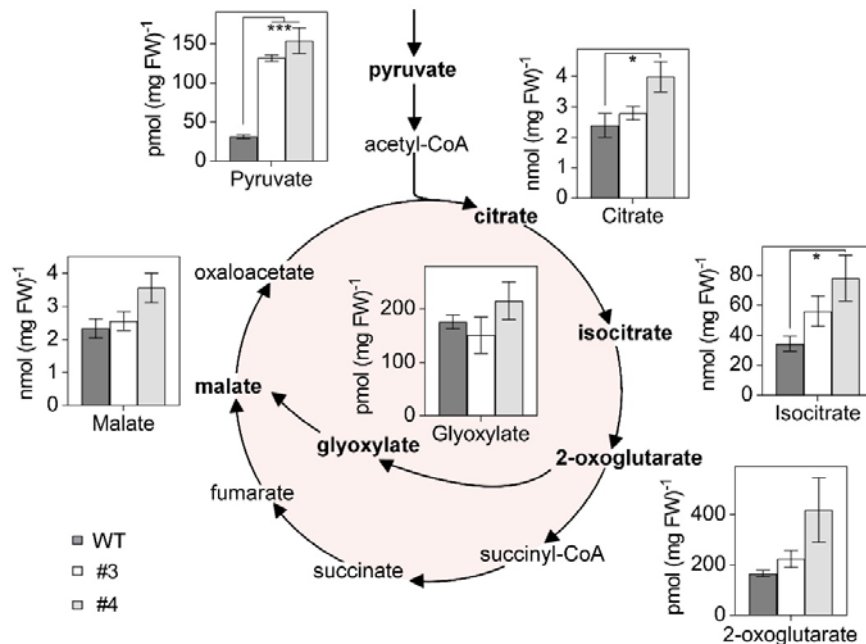
465 **C:** Ratiometric analysis of the E_{GSH}-sensitive fluorescent reporter roGFP2-hGrx1 in mitochondria.
 466 Ratiometric analysis was performed with 7-d-old seedlings of WT and *GRXS15 K83A* lines #3 and #4
 467 expressing mitochondrial roGFP2-hGrx1 by CLSM. For estimation of the dynamic range of the sensor,
 468 wild-type seedlings were incubated in 10 mM DTT (grey squared) or 10 mM H₂O₂ (white squared) and
 469 fluorescence of roGFP2 in the root tips was analyzed. Ratios were calculated from fluorescence images
 470 of cotyledons and root tips of 7-d-old seedlings from two independent reporter lines for each genetic
 471 background ($n = 10$; means \pm SD).

472 **D:** Representative false color images of cotyledons of 7-d-old seedlings show the oxidation state of
 473 roGFP2-Orp1 or roGFP2-hGrx1 targeted to the mitochondrial matrix in WT and *GRXS15 K83A* lines #3
 474 and #4. Bar, 20 μ m.

475 Diminished GRXS15 activity leads to accumulation of TCA cycle intermediates

476 To investigate any other metabolic defects in the GRXS15 K83A mutant, we measured
 477 the concentrations of several organic acids in the *GRXS15 K83A* mutants. We found each of the
 478 analyzed organic acids in the complemented *grxs15* mutants #3 and #4 to be increased.
 479 Pyruvate showed the most pronounced change, increasing by more than four-fold from $31.5 \pm$
 480 $2.4 \text{ pmol (mg FW)}^{-1}$ in the WT to 131.76 ± 3.8 and $153.97 \pm 16.5 \text{ pmol (mg FW)}^{-1}$ in line #3 and
 481 #4 (Fig. 6). The accumulation of citrate and isocitrate was significant in line #4, but not in line
 482 #3. 2-oxoglutarate and malate showed minor increases in line #3 and pronounced increases in
 483 line #4. This trend did not reach statistical significance, however. A similarly concerted
 484 accumulation of TCA cycle intermediates was previously observed in antisense lines of the
 485 mitochondrial manganese superoxide dismutase 1 (MSD1) (Morgan et al., 2008). Those lines
 486 showed impaired mitochondrial ACO activity to less than 50%, suggesting that the compromised
 487 ACO activity is sufficient as an explanation for the rearrangements in the pools of TCA cycle
 488 intermediates. However, pyruvate content was not determined in the *MSD1 antisense* lines and
 489 the increased pyruvate content found in *GRXS15 K83A* lines cannot be straightforwardly linked
 490 to ACO activity.

491



492

493 Figure 6. Organic acids of the TCA cycle accumulate in *Arabidopsis GRXS15 K83A* mutants.

494 Organic acids were analyzed in 8-d-old seedlings of WT compared to *GRXS15 K83A* lines #3 and #4
 495 ($n = 4-5$; means \pm SEM). The statistical analysis (one-way ANOVA with post hoc Holm-Sidak
 496 comparisons for WT vs. mutant lines) indicated significant changes; *: $P \leq 0.05$; ***: $P \leq 0.001$.

497

498 **Alterations in pyruvate and glycine metabolism are correlated with impairment of lipoyl**
499 **cofactor-dependent enzymes under diminished GRXS15 activity**

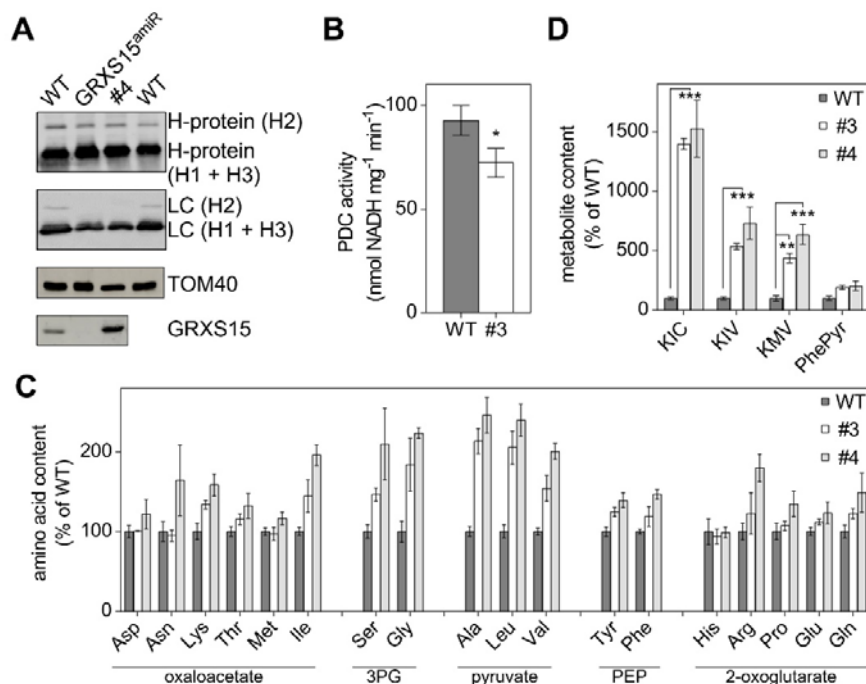
500 The pronounced pyruvate accumulation may be caused by a backlog of metabolites due
501 to a lower TCA flux or by a diminished activity of PDC, which catalyzes the decarboxylation of
502 pyruvate to acetyl-CoA (Yu et al., 2012). The E2 subunit of this multi-enzyme complex uses a
503 lipoyl cofactor, the synthesis of which was shown to be compromised in *GRXS15^{amiR}* mutants
504 (Ströher et al., 2016). In plant mitochondria, the lipoyl moiety is an essential cofactor of four
505 protein complexes: PDC, OGDC, BCKDC, and GDC (Taylor et al., 2004). Ströher et al. (2016)
506 showed decreased lipoylation of PDC E2-2 and E2-3 but no effects on E2-1. On the other hand,
507 a pronounced decrease was observed in all GDC H protein isoforms and differences in the
508 degree of lipoylation were explained by different modes of lipoylation. To get insight into the
509 metabolic effects of diminished GRXS15 activity, we tested for protein lipoylation in the weakest
510 complementation line #4 and directly compared the results to lipoylation in *GRXS15^{amiR}* and WT.
511 Furthermore, the complementation lines #3 and #4 were characterized for metabolites
512 dependent on lipoyl cofactor-dependent enzymes. Immunodetection of the lipoyl group with
513 specific antibodies to the cofactor indicated that the amount of lipoate bound to the H subunit
514 isoforms of GDC was decreased in the *GRXS15 K83A* mutant to a similar extent as in
515 *GRXS15^{amiR}* (Fig. 7A). In contrast, the H protein levels were largely unchanged in all tested
516 lines. GRXS15 was barely detectable in *GRXS15^{amiR}* while in line #4 the mutated *GRXS15*
517 *K83A* was present at even higher amounts than the endogenous protein in wild-type plants.

518 To further test whether the accumulation of pyruvate was due to a less active PDC, we
519 measured the activity of the PDC in isolated mitochondria. Interestingly, there was a 22%
520 reduction in activity. While the WT had a PDC activity of 92.7 ± 6.5 nmol NADH $\text{mg}^{-1} \text{min}^{-1}$ the
521 *GRXS15 K83A* line #3 had a significantly lower activity of only 72.40 ± 6.2 nmol NADH $\text{mg}^{-1} \text{min}^{-1}$
522 (Fig. 7B).

523 The pronounced increase of pyruvate and several TCA intermediates (Fig. 6) may have
524 further effects on downstream metabolites. Given that intermediates of glycolysis and the TCA
525 cycle are hubs for synthesis of amino acids and because mutants defective in PDC subunit E2
526 show an increase in the pools of nearly all amino acids (Yu et al., 2012), we profiled the
527 abundance of amino acids. Most amino acids were increased in the mutants compared to WT
528 seedlings, with more pronounced increases in line #4 compared to line #3 (Fig. 7C,
529 Supplemental Table S1). Particularly high increases in amino acid abundance of more than
530 200% were observed for glycine and serine derived from 3-phosphoglycerate, for alanine,
531 leucine and valine all derived from pyruvate, and for isoleucine (Fig. 7C, Supplemental Table
532 S1). The Gly/Ser ratio, indicative of photorespiratory effects, did not show any pronounced

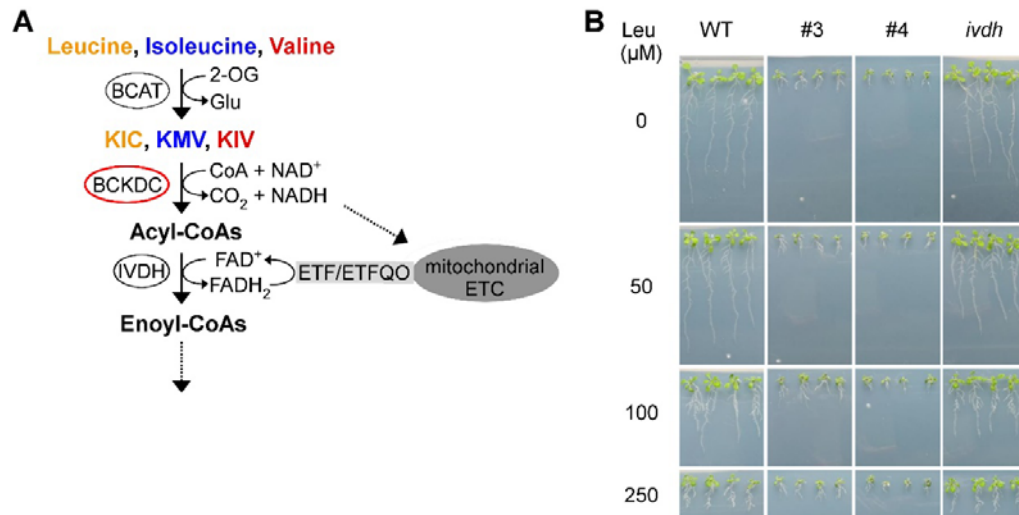
533 change and varied only between 0.33 ± 0.04 for the WT, 0.4 ± 0.1 for line #3 and 0.37 ± 0.12 for
 534 line #4.

535



536

537 **Figure 7. Lipoyl cofactor-dependent enzymes are affected in Arabidopsis *GRXS15* K83A mutants.**
 538 **A:** Immunoblot analysis using antibodies against glycine dehydrogenase H-protein (H1-3), lipoyl cofactor
 539 (LC) as well as antibodies against TOM40 for a loading control and GRXS15. 15 µg of isolated
 540 mitochondria were loaded per lane.
 541 **B:** Pyruvate dehydrogenase complex (PDC) activity in isolated mitochondria. Reduction of NAD⁺ was
 542 measured in mitochondria isolated from 14-d-old seedlings of WT and the *GRXS15* K83A line #3 ($n = 5$;
 543 means \pm SEM). The statistical analysis (one-way ANOVA with post hoc Holm-Sidak comparisons for WT
 544 vs. *grxs15* mutant) indicated significant changes; * $P \leq 0.05$.
 545 **C:** Relative abundance of amino acids in 8-d-old seedlings of WT compared *GRXS15* K83A lines #3 and
 546 #4. WT was set to 100% ($n = 4-5$, means \pm SEM). Absolute values and statistical analysis are provided in
 547 Suppl. Table S1. Amino acids were categorized after their respective common precursor. 3PG = 3-
 548 phosphoglycerate, PEP = phosphoenolpyruvate.
 549 **D:** Analysis of the breakdown products of leucine, isoleucine and valine – α -ketoisocaproic acid (KIC), α -
 550 ketoisovaleric acid (KIV), α -keto- β -methylvaleric acid (KMV) – and phenylpyruvate (PhePyr) in seedlings
 551 of WT compared to *GRXS15* K83A lines #3 and #4. WT was set to 100% ($n = 4-5$; means \pm SEM).
 552 Absolute values are provided in Suppl. Table S1. The statistical analysis (two-way ANOVA with post hoc
 553 Holm-Sidak comparisons for WT vs. *grxs15* mutant) indicated significant changes; ** $P \leq 0.01$;
 554 *** $P \leq 0.001$.
 555
 556



557

558 **Supplemental Figure S5. Catabolism of branched-chain amino acids in Arabidopsis seedlings.**

559 **A:** The branched-chain amino acids leucine, isoleucine and valine are deaminated by branched-chain
560 aminotransferase (BCAT), which uses largely 2-oxoglutarate (2-OG) forming the branched-chain keto
561 acids α -ketoisocaproic acid (KIC), α -keto- β -methylvaleric acid (KMV) and α -ketoisovaleric acid (KIV) as
562 well as glutamate. The keto acids are further degraded by branched-chain keto acid dehydrogenase
563 (BCKDC), which catalyzes the oxidative decarboxylation producing thereby acyl-CoA and NADH.
564 Isovaleryl-CoA dehydrogenase (IVDH) catalyzes the third step providing electrons to the electron
565 transport chain (ETC) via electron transfer flavoprotein (ETF)/electron transfer flavoprotein ubiquinone
566 oxidoreductase (ETFQO) (modified after Peng et al. (2015)).

567 **B:** Leucine sensitivity of WT, *GRXS15 K83A* lines #3 and #4 and *ivdh* mutants. 4-d-old seedlings were
568 transferred to plates containing the respective leucine amount and were analyzed after 7 d.

569

570

571 **Branched-chain amino acid metabolism is strongly impaired in response to diminished**
572 **GRXS15 activity and lipoyl cofactor availability**

573 Leucine, valine and isoleucine are classified as BCAAs, which share a common
574 degradation pathway that is localized in the mitochondrion. Because the BCAA catabolism
575 pathway involves lipoyl cofactor--dependent BCKDC, the increase in the pools of all three
576 BCAAs may not exclusively result from increased availability of their parent compounds, but
577 also from restricted BCAA degradation capacity. To test this hypothesis, we measured the
578 content of the respective keto acids resulting from deamination of the BCAAs by branched-chain
579 amino acid transaminase (BCAT; Supplemental Fig. 5A). The keto acids α -ketoisocaproic acid
580 (KIC), α -keto- β -methylvaleric acid (KMV) and α -ketoisovaleric acid (KIV) derived from the
581 BCAAs accumulated massively in both *GRXS15 K83A* mutants (Fig. 7D). Here, KIC
582 accumulated in the *GRXS15 K83A* mutants up to 15-fold, resulting in values of 3.5 ± 0.11 pmol
583 (mg FW)⁻¹ in line #3 and 3.8 ± 0.6 pmol (mg FW)⁻¹ in line #4 compared to 0.25 ± 0.032 pmol
584 (mg FW)⁻¹ in the WT. KIV and KMV increased 6 to 7-fold in the *GRXS15 K83A* mutants. These

585 pronounced changes support the hypothesis of decreased BCKDC activity creating a bottleneck
 586 in keto acid catabolism (Supplemental Fig. S5A). The higher accumulation of KIC can be
 587 accounted for by the preference of BCKDC for the Val derivative (Taylor et al., 2004) resulting in
 588 KIV to be metabolized faster and to accumulate less strongly. Despite the presumed bottleneck
 589 in catabolism of BCAAs, the *grxs15* mutants did not show enhanced Leu sensitivity
 590 (Supplemental Fig. S5B). Similarly, *ivdh* mutants deficient in isovaleryl-CoA dehydrogenase did
 591 not display an increased sensitivity to external supply of Leu compared to WT.

592

593 **Supplementary Table S1. Content of amino acids and keto acids of Arabidopsis WT and GRXS15**
 594 **K83A lines #3 and #4.** The statistical analysis (two-way ANOVA with post hoc Holm-Sidak comparisons
 595 for WT vs. *grxs15* mutant) indicated significance levels; * $P \leq 0.1$, ** $P \leq 0.01$; *** $P \leq 0.001$; ns: not
 596 significant.
 597

Amino acid	amount of amino acid (pmol (mg FW) ⁻¹); mean ± SEM (% compared to WT; significance level)		
	WT	#3	#4
Ala	96.66 ± 6.2	206.49 ± 15.25 (213.6; ***)	237.99 ± 21.35 (246.2; ***)
Leu	6.48 ± 0.53	13.32 ± 1.36 (205.5; ***)	15.55 ± 1.3 (239.8; ***)
Gly	36.79 ± 4.84	67.70 ± 12.19 (184.0; ***)	82.26 ± 2.38 (223.6; ***)
Ser	111.74 ± 9.6	163.90 ± 9.11 (146.7; *)	234.56 ± 50.21 (209.9; ***)
Val	16.48 ± 0.72	25.45 ± 2.63 (154.5; *)	33.03 ± 1.64 (200.5; ***)
Ile	5.45 ± 0.29	7.89 ± 1.1 (144.7; *)	10.70 ± 0.7 (196.3; ***)
Arg	9.96 ± 1.07	12.22 ± 2.56 (122.7; ns)	17.94 ± 1.72 (180.1; ***)
Asn	76.35 ± 9.27	72.38 ± 5.36 (94.8; ns)	125.24 ± 33.73 (164.0; **)
Lys	6.61 ± 0.65	8.85 ± 0.36 (133.9; ns)	10.49 ± 0.9 (158.6; *)
Gln	213.64 ± 17.12	262.03 ± 13.91 (122.7; ns)	317.91 ± 52.1 (148.8; *)
Phe	6.32 ± 0.18	7.49 ± 0.8 (118.6; ns)	9.26 ± 0.36 (146.6; ns)
Tyr	1.50 ± 0.09	1.87 ± 0.08 (124.9; ns)	2.09 ± 0.14 (139.2; ns)
Pro	31.51 ± 3.24	33.73 ± 1.87 (107.0; ns)	42.39 ± 5.11 (134.5; ns)
Thr	58.94 ± 3.66	68.05 ± 4.03 (115.5; ns)	77.90 ± 9.11 (132.2; ns)
Glu	652.08 ± 32.85	730.33 ± 22.23 (112.0; ns)	805.71 ± 90.0 (123.6; ns)
Asp	199.61 ± 15.02	200.89 ± 1.35 (100.6; ns)	243.28 ± 37.33 (121.9; ns)
Met	1.48 ± 0.07	1.44 ± 0.12 (97.3; ns)	1.72 ± 0.12 (116.7; ns)
His	13.46 ± 2.15	12.67 ± 1.24 (94.1; ns)	13.32 ± 0.91 (99.0; ns)
Keto acid	amount of keto acid (pmol (mg FW) ⁻¹); mean ± SEM (% compared to WT; significance level)		
KIC	0.25 ± 0.03	3.52 ± 0.12 (1396.7 ± 45.8; ***)	3.84 ± 0.60 (1525.3 ± 238.2; ***)
KIV	0.39 ± 0.05	2.10 ± 0.10 (534.7 ± 25.7; ***)	2.88 ± 0.54 (731.5 ± 136.2; ***)
KMV	0.14 ± 0.03	0.61 ± 0.06 (436.9 ± 39.6; ***)	0.89 ± 0.12 (636.4 ± 82.7; ***)

598

599

600

601 Discussion

602 GRXS15 function limits growth

603 Null mutants of mitochondrial GRXS15 are embryo-defective but can be partially
604 complemented with a mutated GRXS15 protein compromised in its ability to coordinate a [2Fe-
605 2S] cluster (Moseler et al., 2015). The bottleneck in Fe-S coordination results in a dwarf
606 phenotype similar to the phenotype of severe knockdown mutants generated through
607 expression of artificial microRNAs (Supplemental Fig. S1) (Ströher et al., 2016) but how exactly
608 the modification of either activity or abundance of GRXS15 impacts on plant growth and
609 development remained unclear. Less severe knockdown mutants resulting from a T-DNA
610 insertion in the 5'-UTR of *GRXS15* limited the abundance of GRXS15 to about 20% of WT
611 levels, but did not show a macroscopic phenotype beyond early seedling stage under non-
612 stress conditions (Ströher et al., 2016). The growth phenotype of more severe *grxs15* mutants is
613 most apparent in very short roots, which may be linked to the fact that *GRXS15* is strongly
614 expressed in roots, particularly in the maturation and meristematic zone (Belin et al., 2015). The
615 primary function of GRXS15 is assumed to be a role in mitochondrial Fe-S cluster transfer
616 (Moseler et al., 2015; Ströher et al., 2016). This implies that a compromised GRXS15 function
617 potentially may have implications for Fe-S-dependent pathways, including biosynthesis of biotin
618 and Moco, the mETC, and the TCA cycle. While biotin feeding experiments clearly excluded
619 biotin biosynthesis as the limiting factor, the picture was less clear for Moco, which is an
620 essential cofactor for several cytosolic enzymes (Schwarz and Mendel, 2006). Nitrate
621 assimilation, which is dependent on Moco-containing nitrate reductase, initially showed the
622 expected nitrate sensitivity. Measurements of extractable nitrate reductase activity, however,
623 showed no defects. Because, similarly xanthine dehydrogenase and aldehyde oxidases did not
624 show changes in their activities between mutants and the WT, deficiencies in Moco supply can
625 be excluded as a putative metabolic bottleneck in *GRXS15 K83A* mutants. Nitrate sensitivity in
626 *grxs15* mutants leaves us with the conundrum of a different link between mitochondrial functions
627 of GRXS15 and nutrient assimilation, which deserves further investigation in the future.

628

629 GRXS15 does not affect energy balance and ROS levels

630 Diminished growth correlates with decreased root respiration rates in both, severe
631 *GRXS15^{amiR}* knockdown mutants (Ströher et al., 2016) and the weak complementation line #3
632 investigated in this work (Fig. 4A). Because the mETC contains 12 Fe-S proteins involved in
633 electron transport (Couturier et al., 2015; Meyer et al., 2019) restricted supply of Fe-S clusters
634 would be expected to affect electron flow along the mETC. In humans, it was observed that a
635 patient deficient in mitochondrial glutaredoxin 5 (GLRX5) suffers from decreased abundance

636 and hence activity of complex I (Ye et al., 2010). In yeast, $\Delta grx5$ mutants displayed a decreased
637 complex II activity, albeit an unaffected protein abundance in this complex (Rodríguez-
638 Manzaneque et al., 2002). In contrast, we found no changes in abundance of any mETC
639 complexes in severe *grxs15* mutants of Arabidopsis (Fig. 4B). Consistently, feeding of
640 mitochondria isolated from *GRXS15 K83A* mutants with succinate revealed that SDH, which
641 contains three different Fe-S clusters (Figueroa et al., 2001), does not constitute a bottleneck in
642 mitochondrial metabolism of *grxs15* mutants. Generally, the respiratory capacity is not affected
643 in the mutants compared to WT, which indicates that supply of Fe-S clusters to components of
644 the mETC is not compromised in *grxs15* mutants. The lower respiratory rate in *GRXS15 K83A*
645 mutants also does not lead to changes in ATP levels. This, however, may also partially be due
646 to decreased consumption of ATP with restricted growth and also the activity of adenylate
647 kinase that contributes to formation of ATP (and AMP) from ADP to buffer the ATP level (De Col
648 et al., 2017). Our overall conclusion to this point is that reduced respiration is likely due to
649 restricted substrate supply rather than assembly of complexes in the mETC and their supply
650 with Fe-S clusters. Restricted supply of reducing equivalents may result from a slowdown of the
651 TCA cycle and also from severely compromised contributions of the electron-transfer
652 flavoprotein/electron-transfer flavoprotein:ubiquinone oxidoreductase (ETF/ETFQO) to
653 ubiquinone reduction (Supplemental Fig. S5). Electrons that enter the mETC via ETF/ETFQO
654 originate from IVDH mediated oxidation of acyl-CoAs as products of BCKDC. The ETF/ETFQO
655 pathway has been shown to contribute significant amounts of electrons in stress situations
656 (Ishizaki et al., 2005; Pires et al., 2016). The concomitant increase in BCKAs and particularly
657 BCAAs may contribute to the dwarf phenotype as disruption in BCAA homeostasis has been
658 shown to lead to pleiotropic effects including growth retardation (Cao et al., 2019).

659

660 **GRXS15 affects enzymes and metabolites in the TCA cycle**

661 GRXS15 was detected as part of higher order protein assemblies in a mitochondrial
662 complexome analysis (Senkler et al., 2017). A particularly strong interaction between GRXS15
663 and mitochondrial isocitrate dehydrogenase 1 (IDH1) was observed in yeast two-hybrid screens
664 with IDH1 as bait and this interaction was subsequently confirmed by bimolecular fluorescence
665 (BiFC) assays (Zhang et al., 2018). Consistent with a suspected role of GRXS15 in IDH1
666 function, the isocitrate content was decreased significantly in a *grxs15* knockdown mutant, while
667 the relative flux through the TCA cycle increased (Zhang et al., 2018). IDH1 has recently been
668 reported to contain several redox-active thiols that can change their redox state depending on
669 substrate availability for the TCA (Nietzel et al., 2020). The IDH1-GRXS15 interaction thus could
670 point at a possible function of GRXS15 as a thiol-switch operator for regulatory thiols. This is
671 unlikely though, because GRXS15 does not show any reductive activity and only weak oxidative

672 activity (Moseler et al., 2015; Begas et al., 2017). The increase in all analyzed metabolites of the
673 TCA cycle is rather consistent with metabolite patterns found in knockdown mutants of
674 mitochondrial MnSOD, in which increased levels of organic acids correlated with a decrease in
675 ACO activity (Morgan et al., 2008). Aconitase contains a [4Fe-4S] cluster and has frequently
676 been used as an enzymatic marker for defects in Fe-S cluster assembly and transfer in yeast
677 and human cells (Rodríguez-Manzanaque et al., 2002; Bandyopadhyay et al., 2008; Liu et al.,
678 2016). It came as a surprise that ACO was reported to be unaffected in mitochondria of
679 *Arabidopsis grxs15* mutants, both in abundance and activity (Ströher et al., 2016). Consistent
680 with this report, we also found no change in abundance of mitochondrial ACOs, but did find
681 reduced activity (Fig. 5). This decrease in activity may well reflect decreased supply of [4Fe-4S]
682 in line with reports for mutants from non-plant species with defects in mitochondrial Fe-S
683 transfer (Rodríguez-Manzanaque et al., 2002; Liu et al., 2016). In addition, ACOs are prone to
684 oxidative modification by ROS or reactive nitrogen species (Castro et al., 2019) and indeed
685 redox-sensitive thiol residues have been identified on mitochondrial ACOs as putative thiol
686 switches (Nietzel et al., 2020). The absence of any detectable oxidative response, however,
687 provides no lead for further investigation of such speculative redox-dependent regulation of
688 ACO activity under non-stress conditions. The decrease in mitochondrial ACO activity in
689 *GRXS15 K83A* mutants does not explain the most pronounced increase in pyruvate, which
690 accumulates up to five-fold and thus supersedes the accumulation of all other TCA cycle
691 intermediates at least by a factor of two. A knockdown of mitochondrial and cytosolic ACO
692 activities in wild tomato led to a reduction in 2-OG levels but an increase in citrate and isocitrate
693 by 40-50%. A similar change in these organic acids of the TCA cycle were found in a succinate
694 dehydrogenase mutant (Carrari et al., 2003; Huang et al., 2013). The pattern of organic acids in
695 *GRXS15 K83A* mutants is thus clearly different from other TCA cycle mutants. The most
696 pronounced increases in pools of 2-OG and pyruvate compared to WT point at diminished
697 activities of PDC and OGDC instead.

698

699 **GRXS15 has a function in protein lipoylation**

700 PDC and OGDC do not contain an Fe-S cluster but rather belong to a class of four
701 dehydrogenase complexes that all involve lipoylated subunits. Lipoylation of mitochondrial
702 proteins is mediated through coordinated action of lipoate-protein ligase, octanoyltransferase,
703 and LIP1 (Ewald et al., 2014). The radical S-adenosylmethionine enzyme LIP1, contains two
704 [4Fe-4S] clusters one of which is required as a substrate, i.e. as sulfur donor to octanoyl-
705 residues (McCarthy and Booker, 2017). Continuous destruction of Fe-S clusters during
706 lipoylation may thus render lipoyl cofactor-dependent-enzymes indirectly sensitive to defects in
707 Fe-S supply. Decreased lipoylation of GDC-H proteins and reduced PDC activity are fully

708 consistent with previous observations on *GRXS15^{amiR}* mutants by Ströher et al. (2016). Similar
709 to the Arabidopsis mutants also humans carrying mutations in mitochondrial GLRX5 are
710 deficient in lipoylation of mitochondrial proteins (Baker et al., 2014). A critical restriction through
711 lipoylation deficiency is further supported by increased amounts of pyruvate and 2-OG as well
712 as several other organic acids and amino acids derived from these precursors (Figs. 6 and 7C).
713 Similar increases in pyruvate as well as the accumulation of most amino acids were also shown
714 for Arabidopsis plants with a mutated PDC-E2 subunit resulting in only 30% PDC activity (Yu et
715 al., 2012). A much more pronounced increase of alanine in PDC-E2 mutants than in *GRXS15*
716 *K83A* mutants may be attributed to a higher severity of the metabolic bottleneck if PDC activity
717 is down to 30%. Of all metabolites analyzed in this study, the 4 to 15-fold increases of BCKAs in
718 *GRXS15 K83A* mutants were the most pronounced relative changes compared to the WT. The
719 findings that these increases were stronger in more severe mutants, point at BCKDC as a
720 critical bottleneck. The keto acids KIC, KIV and KMV are products of transamination of the
721 BCAAs leucine, isoleucine and valine (Hildebrandt et al., 2015). Further degradation of the keto
722 acids in *GRXS15 K83A* mutants is limited because BCKDC relies on efficient lipoylation of the
723 E2 subunit. Like GDC, PDC and OGDC, BCKDC consists of different subunits, which may not
724 be present in stoichiometric amounts. Recently, Fuchs et al. (2020) reported quantitative data
725 for the abundance of proteins in single mitochondria (Fig. 8). These data indicate low
726 abundance of BCKDC-E2 compared to GDC-H and particularly PDC-E2. Given that all four
727 dehydrogenase complexes rely on the same dihydrolipoyl dehydrogenase subunits, i.e. E3 or L
728 subunits, it is obvious that the relative abundance of subunit proteins will have some impact on
729 assembly of functional complexes. With the assumption that all different E2 and H subunits
730 compete with each other and with the same chance of getting lipoylated, the absolute number of
731 lipoylated PDC-E2 proteins is expected to be higher than that of BCKDC-E2 proteins. If even
732 non-lipoylated E2 or H formed complexes with E3 or L, very little functional BCKDC could be
733 formed. Furthermore, the very low copy number of BCKDC-E1 subunits compared to BCKDC-
734 E2 implies that under lipoyl cofactor-limiting conditions, E1 subunits are more likely to form
735 complexes with non-lipoylated and hence non-catalytic E2. *Vice versa*, the few E2 copies that
736 do get lipoylated may not be those that assemble with E1 subunits to form active complexes.
737 Selective transcriptional upregulation of several nominally lipoylated subunits in *GRXS15^{amiR}* as
738 reported by Ströher et al. (2016) would additionally increase the imbalance and tighten the
739 metabolic bottleneck even further.

740 LIP1 was estimated to be present with 85 copies in a single mitochondrion compared to
741 4200 copies of ACO2 and 9900 copies of ACO3 (Fig. 8) (Fuchs et al., 2020). In the absence of
742 any other evidence all apoproteins have a similar likelihood of receiving a [4Fe-4S] cluster. The
743 few LIP1 proteins will have a low chance of receiving a cluster if efficient supply of [2Fe-2S]
744 clusters by *GRXS15* further upstream in the Fe-S cluster transfer machinery is compromised.

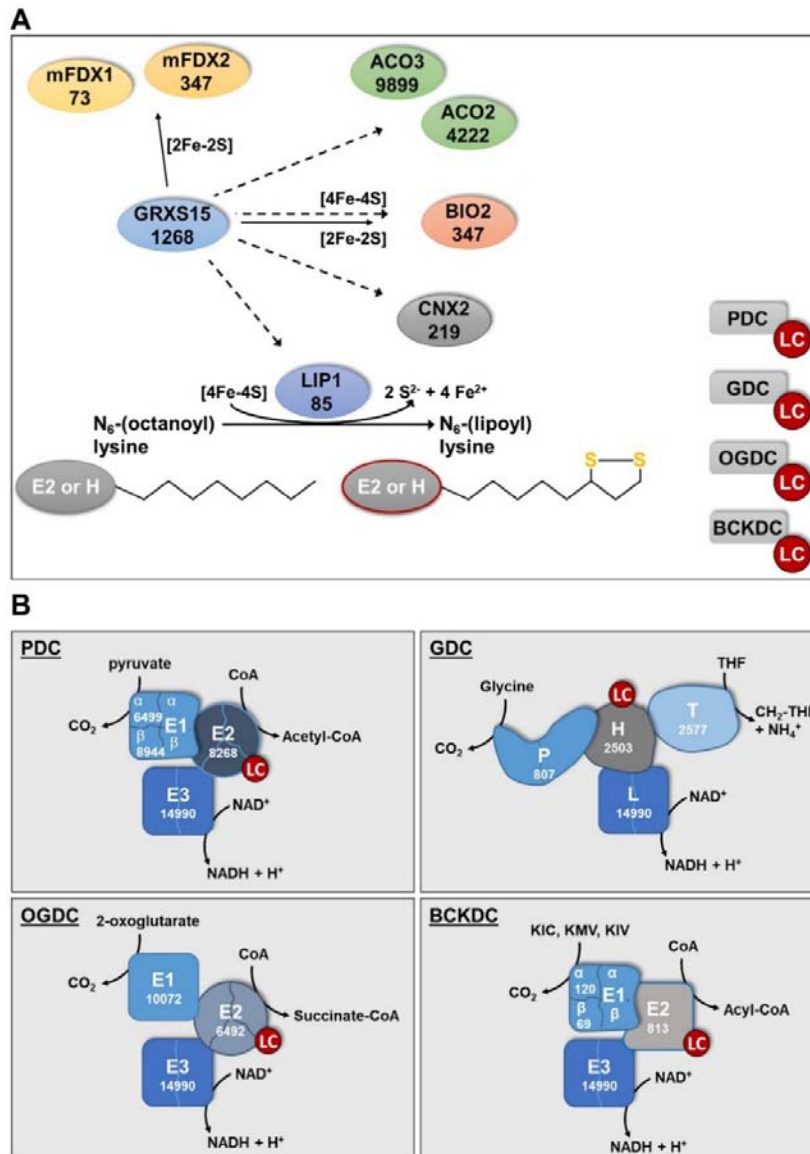
745 With the need for two [4Fe-4S] clusters of which one has to be replaced after each catalytic
746 cycle the bottleneck is bound to become even more severe than in enzymes that use their Fe-S
747 clusters only for electron transfer reactions.

748

749 **Conclusion**

750 We show that compromising the ability of GRXS15 to coordinate and transfer [2Fe-2S]
751 clusters results in severe defects only in enzymes relying on the prosthetic group lipoamide.
752 These results are in agreement with findings by Ströher et al. (2016) who reported diminished
753 lipoylation of proteins in *GRXS15^{amiR}* lines and hypothesized that diminished respiration and the
754 short root mutant phenotype could be a consequence of the incomplete lipoyl cofactor loading
755 of important TCA cycle enzymes. Here we expand and specify the picture, by systematically
756 probing for metabolic bottlenecks in mitochondrial pathways that rely on the supply with Fe-S
757 clusters. While changes in a several metabolites were found, the primary defects can be
758 assigned to merely the four mitochondrial dehydrogenase complexes all of which contain a
759 lipoylated subunit. Those results emphasize the importance of LIP1 as a major sink for Fe-S
760 clusters, which becomes manifest if GRXS15-mediated Fe-S cluster transfer between the
761 assembly machinery and receiving apoproteins is restricted. The fact that most other Fe-S-
762 dependent pathways are not seriously affected by deficiencies in *GRXS15 K83A*
763 complementation lines may be explained by the effective relative abundance of different
764 proteins in mitochondria. We propose that an increased demand for Fe-S as sulfur donor
765 combined with the very low abundance of LIP1 leads to the manifestation of a potentially lethal
766 bottleneck. The phenotype highlights the importance of an accurate maintenance of protein
767 amounts and appropriate stoichiometries for normal mitochondrial function.

768



769

770 **Figure 8. Lipoylation of mitochondrial proteins depends on GRXS15.**

771 **A:** Distribution of Fe-S clusters in Arabidopsis mitochondria to soluble Fe-S proteins and lipoylation of
 772 proteins via lipoyl synthase (LIP1). Putative transfer of Fe-S clusters is indicated by solid arrows for [2Fe-
 773 2S] and dashed arrows for [4Fe-4S]. Intermediate complexes of Fe-S transfer and assembly of [4Fe-4S]
 774 clusters are not shown. mFDX1/2: mitochondrial ferredoxin 1/2; ACO2/3; aconitase 2/3; BIO2: biotin
 775 synthase 2; CNX2: GTP-3',8-cyclase PDC: pyruvate decarboxylase complex; OGDC: 2-oxoglutarate
 776 dehydrogenase complex; GDC: glycine decarboxylase complex; BCKDC: branched-chain α -keto acid
 777 dehydrogenase complex; LC: Lipoyl cofactor. Numbers give the estimated copy number of the respective
 778 proteins according to Fuchs et al. (2020).

779 **B:** Abundance of subunits in the four mitochondrial dehydrogenase complexes PDC, GDC, OGDC and
 780 BCKDC according to Fuchs et al. (2020). The copy number for the H subunit of GDC is only for the
 781 isoform H2, because the nominally more abundant isoforms H1 and H3 (see Fig. 7A) were not identified
 782 by Fuchs et al. (2020). E3 and L subunits are formed by the closely related and highly similar proteins
 783 mtLPD1 (4876 copies) and mtLPD2 (10114 copies), The total of both isoforms is given but it should be
 784 noted that a preference of GDC for mtLPD1 and of the other three complexes for mtLPD2 has been
 785 proposed (Lutziger and Oliver, 2001). Deficiencies of these enzymes generates metabolic bottlenecks
 786 and causes an increase of their respective substrates and particularly for PDC and OGDC also a severe
 787 limit in carbon supply to the TCA cycle.

788 **Material and Methods**

789 **Plant Material & Methods**

790 Previously described *Arabidopsis thaliana* complementation lines *grxs15-3*
791 *UBQ10_{pro}:GRXS15 K83A* (Moseler et al., 2015) and the knock-down line *GRXS15^{amiR}* (Ströher
792 et al., 2016) as well as *atm3-1* and *atm3-4* (Teschner et al., 2010) were used in this study. *A.*
793 *thaliana* ecotype Col-0 ([L.] Heyn.) segregated from the T-DNA line *grxs15-3*) was used as WT.
794 Unless stated differently, surface-sterilized seeds were grown on vertical plates containing
795 nutrient medium (Meyer and Fricker, 2000) with 0.1% (w/v) sucrose solidified with 0.8% (w/v)
796 agar under long-day conditions with a diurnal cycle of 16 h light at 22°C and 8 h dark at 18°C.
797 The light intensity was 75 $\mu\text{E m}^{-2} \text{s}^{-1}$ and 50% air humidity.

798 Germination rate was scored by observing radical emergence in seeds plated on vertical
799 culture plates using a stereomicroscope (Leica M165 FC). Root growth was documented
800 photographically on vertical culture plates containing 0.8% (w/v) phytigel and 0.1% (w/v)
801 sucrose. Five and 8 d after stratification, root length was documented and measured using
802 Adobe Illustrator CS5.1.

803 Influence of the nitrogen source on root length was analyzed on plates containing 5 mM
804 KNO_3 or 2.5 mM $(\text{NH}_4)_2\text{SO}_4$, 2.5 mM KH_2PO_4 , 2 mM MgSO_4 , 2 mM CaCl_2 , 50 μM Fe-EDTA,
805 70 μM H_3BO_4 , 14 μM MnCl_2 , 0.5 μM CuSO_4 , 1 μM ZnSO_4 , 0.2 μM NaMoO_4 , 10 μM NaCl,
806 0.01 μM CoCl_2 , 0.8% (w/v) phytigel and 0.1% (w/v) sucrose, pH 5.8. To check for possible
807 effects of counter anions, $(\text{NH}_4)_2\text{SO}_4$ was replaced by NH_4Cl and grown otherwise exactly under
808 the same conditions.

809 **Blue Native Page**

810 Mitochondrial samples were solubilized in 1% (w/v) n-dodecyl β -D-maltoside and
811 subjected to Blue-Native-PAGE as described previously (Meyer et al., 2011; Kühn et al., 2015).

812 **Isolation of mitochondria**

813 *Arabidopsis* mitochondria were purified from 2- or 4-week-old seedlings as described
814 before (Sweetlove et al., 2007) with slight modifications. All steps were performed on ice or at
815 4°C. Seedlings were homogenized using mortar and pestle and the homogenate was filtered
816 (Miracloth; Merck Millipore) before cellular debris was pelleted by centrifugation for 5 min at
817 1,200 *g*. The supernatant was centrifuged for 20 min at 18,000 *g*, and the pellet of crude
818 mitochondria was gently resuspended in wash buffer (0.3 M sucrose, 0.1% (w/v) BSA and
819 10 mM TES, pH 7.5) and centrifuged for 5 min at 1,200 *g*. The supernatant was transferred into
820 a new tube and centrifuged for 20 min at 18,000 *g*. The pellet was gently resuspended in final
821 wash buffer (0.3 M sucrose, 10 mM TES, pH 7.5), loaded directly on a 0–6% Percoll gradient

822 and centrifuged for 40 min at 40,000 *g*. Mitochondria were transferred into a new tube and
823 washed three times with final wash buffer (0.3 M sucrose, 10 mM TES pH 7.5).

824 **Respiration Assays**

825 Oxygen consumption of intact Arabidopsis roots and isolated mitochondria was
826 measured in Oxytherm Clark-type electrodes (Hansatech; www.hansatech-instruments.com) as
827 described before (Wagner et al., 2015). Whole roots from seedlings vertically grown on agar
828 plates were cut below the hypocotyl-root junction and assayed in a volume of 1.2 mL containing
829 5 mM KCl, 10 mM MES, and 10 mM CaCl₂, pH 5.8, and after addition of 4 mM KCN and 0.2 mM
830 pGal.

831 O₂ consumption of isolated mitochondria was measured in a volume of 1 mL containing
832 0.3 M mannitol, 10 mM TES-KOH pH 7.5, 5 mM KH₂PO₄, 10 mM NaCl, 2 mM MgSO₄ and 0.1%
833 (w/v) bovine serum albumin. O₂ consumption rate was measured before (blank) addition of
834 mitochondria and after addition of mitochondria or respective substrate (state II; succinate
835 (10 mM succinate, 0.25 mM ATP) or pyruvate/malate (10 mM pyruvate, 10 mM malate, 0.3 mM
836 NAD and 0.1 mM thiamine pyrophosphate), state III; ADP (50 μM ADP). Additionally, O₂
837 consumption rate was analyzed after ADP consumption (state IV) and after addition of 10 μM
838 carbonyl cyanide *m*-chlorophenylhydrazone (CCCP).

839 **Histological detection of reactive oxygen species**

840 For detection of increased H₂O₂ production, leaves were stained with DAB (3, 3-
841 diaminobenzidine) (Thordal-Christensen et al., 1997). Leaves were vacuum-infiltrated in a
842 solution containing 0.1 mg mL⁻¹ DAB, 50 mM potassium phosphate buffer pH 7.6 and 0.1% (v/v)
843 Silwet L-77. After infiltration, the leaves were incubated for 20-24 h in the dark and destained by
844 lactic acid:glycerol:EtOH (1:1:3) for 30 min at 70°C.

845 For histochemical staining of superoxide, NBT (nitro blue tetrazolium) was used
846 (Hoffmann et al., 2013). Leaves were vacuum-infiltrated in a solution containing 0.1 mg mL⁻¹
847 NBT, 50 mM potassium phosphate buffer pH 7.6 and 0.1% (v/v) Silwet L-77. After infiltration the
848 leaves were incubated for 30 min in the dark and destained by lactic acid:glycerol:EtOH (1:1:3)
849 for 30 min at 70°C.

850 **Determination of metabolite levels via HPLC**

851 Aliquots (45-55 mg) of freshly ground plant tissue were used for absolute quantification
852 of amino acid, α-keto acid and organic acid content each.

853 Free amino acids and α-keto acids were extracted with 0.5 mL ice-cold 0.1 M HCl in an
854 ultrasonic ice-bath for 10 min. Cell debris and insoluble material were removed by centrifugation
855 for 10 min at 25,000 *g*. For the determination of α-keto acids, 150 μL of the resulting

856 supernatant were mixed with an equal volume of 25 mM OPD (o-phenyldiamine) solution and
857 derivatised by incubation at 50°C for 30 min. After centrifugation for 10 min, the derivatised keto
858 acids were separated by reversed phase chromatography on an Acquity HSS T3 column
859 (100 mm x 2.1 mm, 1.7 µm, Waters) connected to an Acquity H-class UPLC system. Prior
860 separation, the column was heated to 40°C and equilibrated with 5 column volumes of solvent A
861 (0.1% (v/v) formic acid in 10% (v/v) acetonitrile) at a flow rate of 0.55 mL min⁻¹. Separation of
862 keto acid derivatives was achieved by increasing the concentration of solvent B (acetonitrile) in
863 solvent A (2 min 2% B, 5 min 18% B, 5.2 min 22% B, 9 min 40% B, 9.1 min 80% B and hold for
864 2 min, and return to 2% B in 2 min). The separated derivatives were detected by fluorescence
865 (Acquity FLR detector, Waters, excitation: 350 nm, emission: 410 nm) and quantified using
866 ultrapure standards (Sigma). Data acquisition and processing were performed with the
867 Empower3 software suite (Waters). Derivatisation and separation of amino acids was performed
868 as described by (Yang et al., 2015).

869 Total organic acids were extracted with 0.5 mL ultra-pure water for 20 min at 95°C.
870 Organic acids were separated using an IonPac AS11-HC (2 mm, Thermo Scientific) column
871 connected to an ICS-5000 system (Thermo Scientific) and quantified by conductivity detection
872 after cation suppression (ASRS-300 2 mm, suppressor current 95-120 mA). Prior separation,
873 the column was heated to 30°C and equilibrated with 5 column volumes of solvent A (ultra-pure
874 water) at a flow rate of 0.38 mL min⁻¹. Separation of anions and organic acids was achieved by
875 increasing the concentration of solvent B (100 mM NaOH) in buffer A (8 min 4% B, 18 min 18%
876 B, 25 min 19% B, 43 min 30% B, 53 min 62% B, 53.1 min 80% B for 6 min, and return to 4% B
877 in 11 min). Soluble sugars were separated on a CarboPac PA1 column (Thermo Scientific)
878 connected to the ICS-5000 system and quantified by pulsed amperometric detection (HPAEC-
879 PAD). Column temperature was kept constant at 25°C and equilibrated with five column
880 volumes of solvent A (ultra-pure water) at a flow rate of 1 mL min⁻¹. Baseline separation of
881 carbohydrates was achieved by increasing the concentration of solvent B (300 mM NaOH) in
882 solvent A (from 0 to 25 min 7.4% B, followed by a gradient to 100% B within 12 min, hold for
883 8 min at 100% B, return to 7.4% B and equilibration of the column for 12 min). Data acquisition
884 and quantification was performed with Chromeleon 7 (Thermo Scientific).

885 **Aldehyde oxidase and xanthine dehydrogenase assay**

886 Aldehyde oxidase (AO) and xanthine dehydrogenase (XDH) assays were performed
887 similar as described previously by Koshiha et al. (1996) and Hesberg et al. (2004). For
888 determination of AO and XDH activities Arabidopsis seedlings were homogenized in extraction
889 buffer (0.1 M potassium phosphate buffer pH 7.5, 2.5 mM EDTA and 5 mM DTT) and
890 centrifuged for 10 min at 16,000 g and 4°C. Enzyme activities of AO and XDH in the resulting
891 supernatant were detected after native PAGE by activity staining. Activity of AO was developed

892 in a reaction mixture containing 0.1 M potassium phosphate buffer pH 7.5, 1 mM 1-
893 naphthaldehyde, 1 mM indole-3-carboxaldehyde, 0.1 mM phenazine methosulfate (PMS), and
894 0.4 mM MTT (3-(4,5-dimethylthiazol-2-yl)-2,5-diphenyltetrazolium bromide) at RT. Activity of
895 XDH was analyzed with a staining solution of 1 mM hypoxanthine, 1 mM MTT and 0.1 mM PMS
896 in 250 mM Tris-HCl, pH 8.5.

897 **Nitrate Reductase assay**

898 Nitrate reductase (NR) assay was performed as described previously (Scheible et al.,
899 1997) with slight modifications. Leaves were homogenized in extraction buffer (50 mM MOPS,
900 pH 7.0, 50 mM KCl, 5 mM Mg-acetate, 1 mM CaCl₂, 2 mM Na-citrate and 1 mM DTT) and
901 centrifuged for 10 min at 20,000 *g* and 4°C. NR activity was measured in a reaction mixture
902 containing 50 mM MOPS, pH 7.0, 50 mM KCl, 5 mM Mg-acetate, 1 mM CaCl₂, 10 mM KNO₃
903 and 0.4 mM NADH. At consecutive time points, 150 µL aliquots were removed from the mixture
904 and the reaction was stopped by adding 54 mM zinc acetate and 37.5 µM PMS. Thereafter,
905 0.475% (v/v) sulfanilamide in 1 N HCl and 0.005% (v/v) N-(1-naphthyl)-ethylenediamine was
906 added. Samples were allowed to stand for 15 min at RT in the dark and the absorbance of the
907 produced azo-dye was measured at 540 nm.

908 **Aconitase assay**

909 Aconitase activity was analyzed in a coupled assay measuring NADPH formation by
910 monitoring the increase in absorbance at 340 nm using a plate reader (CLARIOstar®; BMG).
911 The reaction mixture contained 50 mM HEPES pH 7.8, 2.5 mM NADP⁺, 5 mM MnCl₂, 0.1% (v/v)
912 Triton X-100 and 0.05 U isocitrate dehydrogenase. The mixture was allowed to come to
913 equilibrium after addition of protein extract. The reaction was started by adding 8 mM cis-
914 aconitic acid.

915 **Pyruvate dehydrogenase complex assay**

916 To estimate the activity of pyruvate dehydrogenase complex, mitochondria were isolated
917 as described previously and reduction of NAD⁺ was measured at 340 nm in a reaction mixture
918 containing ~10 µg mitochondria in 100 mM MOPS pH 7.4, 1 mM CaCl₂, 1 mM MgCl₂, 4 mM
919 cysteine, 0.45 mM thiamine pyrophosphate, 0.18 mM Coenzyme A, 3 mM NAD⁺ and 0.1% (v/v)
920 Triton X-100. The reaction was started with 7.5 mM pyruvate.

921 **Fatty Acid Methyl Ester (FAME) Measurement**

922 The analysis of fatty acids was performed by quantification of their respective fatty acid
923 methyl esters (FAMES) via gas chromatography coupled with a flame ionization detector as
924 described before (Browse et al., 1986). 1 mL 1 N HCl in MeOH was added to 5 seeds or
925 ~50 mg homogenized seedlings as well as 5 µg pentadecanoic acid as internal standard.
926 Samples were incubated at 80°C for 2 h (seeds) or 30 min (seedlings). After cooling down, 1 mL

927 0.9% (w/v) NaCl and 1 mL hexane were added. Samples were mixed vigorously and centrifuged
928 with 1,000 g for 3 min. The hexane phase was transferred to a GC vial. FAMES were quantified
929 using pentadecanoic acid as internal standard.

930 **Western Blotting**

931 For protein blot analysis, total cell extract or purified organelles were heated for 5 min
932 and separated on standard SDS/PAGE gels. Proteins were transferred to a membrane
933 (BioTrace PVDF Transfer Membrane; Pall Corporation) and labeled with antibodies
934 (Streptavidin HRP: ab7403 Abcam; lipoic acid: ab58724, aconitase: see Bernard et al. (2009).
935 The GRXS15 antibody was a kind gift of Nicolas Rouhier (Nancy) and the H protein antibody a
936 kind gift of Olivier Keech (Umea). The TOM40 antibody was a kind gift of Jim Whelan
937 (Melbourne). Immunolabeling was detected by chemiluminescence by using secondary
938 horseradish peroxidase-conjugated antibodies and Pierce ECL Western Blotting Substrate.

939 **Fluorescence microscopy**

940 Fluorescent plants were selected using a stereomicroscope (Leica M165 FC) equipped
941 with a GFP filter.

942 A confocal laser scanning microscope (Zeiss LSM 780, attached to an Axio
943 Observer.Z1; Carl Zeiss Microscopy) and a ×40 (C-Apochromat, 1.20 numerical aperture, water
944 immersion) or ×63 lens (Plan-Apochromat, 1.40 numerical aperture, oil immersion) was used for
945 confocal imaging. For ratiometric analyses of mitochondrial localized roGFP2-hGrx1 (Albrecht et
946 al., 2014) or roGFP2-Orp1 (Nietzel et al., 2019), lines with similar expression levels in WT and
947 mutants were selected. For both sensors, roGFP2 was excited at 405 and 488 nm. For both
948 excitation wavelengths, roGFP2 fluorescence was collected with a bandpass filter of 505-530
949 nm.

950 The cytosolic ATeam 1.03-nD/nA was excited at 458 nm and emission of CFP
951 (mseCFP) and Venus (cp173-mVenus) was collected at 499-544 nm and 579-615 nm,
952 respectively. Background signal was subtracted before ratiometric analysis.

953 For all emissions, intensities from four scans were averaged. Ratiometric analysis was
954 performed using a custom-written MATLAB script (Fricker, 2016) using x,y noise filtering and
955 fluorescence background subtraction.

956 **Statistical analysis**

957 Statistics and error bars were applied for independent experiments with at least three
958 biological replicates using the program GraphPad Prism 6.

959

960 **Supplemental Data**

961 **Supplemental Figure S1.** Arabidopsis mutants affected in GRXS15 function develop a dwarf
962 phenotype.

963

964 **Supplemental Figure S2.** Moco enzymes and anions are not affected in Arabidopsis
965 *GRXS15 K83A* mutants

966

967 **Supplemental Figure S3.** *In vivo* monitoring of ATP levels in the cytosol of Arabidopsis
968 *GRXS15 K83A* mutants.

969

970 **Supplemental Figure S4.** Analysis of the oxidation state of the Arabidopsis *grxs15* mutants.

971

972 **Supplemental Figure S5.** Catabolism of branched-chain amino acids in Arabidopsis seedlings.

973

974 **Supplementary Table S1.** Content of amino acids and keto acids of Arabidopsis WT and
975 *GRXS15 K83A* lines #3 and #4.

976

977 **Acknowledgements**

978 We would like to thank Elke Ströher and Harvey Millar for providing the knock-down line
979 *GRXS15^{amiR}* as well as Nicolas Rouhier, Olivier Keech and Jim Whelan for providing antibodies.

980 We thank Philippe Fuchs, Stefanie Müller-Schüssele and Nicolas Rouhier for helpful discussion
981 and critical reading of the manuscript.

982

983 **Figure Legends**

984 **Figure 1. Complementation of the Arabidopsis *grxs15-3* mutant with**
985 ***UBQ10_{pro}:GRXS15 K83A*.**

986 **A:** 8-d-old wild-type (WT) seedlings compared with *GRXS15 K83A* mutants grown on vertical
987 agar plates under long-day conditions.

988 **B:** Primary root length of 8-d-old *GRXS15 K83A* mutants compared to WT ($n = 35$;
989 means \pm SD). Different letters indicate significant differences between the different lines;
990 $P \leq 0.05$; (one-way ANOVA with post hoc Holm-Sidak).

991

992

993 **Figure 2. *GRXS15 K83A* mutation has no impact on the biotin pathway in Arabidopsis**
994 **seedlings.**

995 **A:** Immunoblot analysis of biotinylated MCCA in mitochondria of *GRXS15 K83A* mutants
996 compared with WT. In the upper panel, biotinylated MCCA was detected by streptavidin HRP in
997 isolated mitochondria from 2-weeks-old seedlings (9 μ g protein was loaded per lane). In the
998 lower panel, amido black staining of the membrane is shown as a control for protein loading.

999 **B, C:** Fatty acids quantified by gas chromatography using a flame ionization detector of 8-d-old
1000 seedlings (B) and seeds (C) of *GRXS15 K83A* line #4 compared to WT ($n = 3-4$; means \pm SD).
1001 The statistical analysis (two-way ANOVA with post hoc Holm-Sidak comparisons for WT vs.
1002 *grxs15*) indicated no significant ($P \leq 0.05$) change except for 18:3 (***) = $P < 0.001$).

1003 **D:** *GRXS15 K83A* line #4, the knockdown line *GRXS15^{amiR}* (amiR) and wild-type plants were
1004 grown on horizontal plates with $\frac{1}{2}$ MS agar without sucrose. The medium contained either no
1005 biotin (control), 1 μ M biotin or 1 μ M desthiobiotin.

1006

1007

1008 **Figure 3. Growth of Arabidopsis *GRXS15 K83A* mutants is affected by the nitrogen**
1009 **source.**

1010 **A:** Primary root length of *GRXS15 K83A* lines #3 and #4 as well as *atm3-1* seedlings compared
1011 to WT grown on vertical agar plates containing 5 mM KNO_3 or 2.5 mM $(\text{NH}_4)_2\text{SO}_4$ as N-source
1012 for 8 d under long-day conditions ($n = 30$; means \pm SD). Student's t-Test analysis showed
1013 significant differences between the growth on the different inorganic N-sources in all lines ***:
1014 $P < 0.001$.

1015 **B:** Representative 4-week-old plants of WT, *GRXS15 K83A* lines #3 and #4 and *atm3-1* all
1016 grown on soil under long-day conditions. Scale bar = 2 cm.

1017 **C:** Nitrate reductase activity in WT, lines #3 and #4 as well as in *atm3-1*. Activity was analyzed
1018 in 4-week-old plants grown on soil by measuring the presence of nitrite via the Griess reaction
1019 ($n = 4$; means \pm SD, **: $P \leq 0.01$).

1020 **D:** Nitrate and nitrite content of 8-d-old WT and *GRXS15 K83A* lines #3 and #4 seedlings grown
1021 on agar plates ($n = 4$; means \pm SEM). The statistical analysis (two-way ANOVA with post hoc
1022 Holm-Sidak comparisons for WT vs. *grxs15*) indicated a significant change in the nitrate
1023 content; ***: $P \leq 0.001$.

1024 **E:** In-gel activity of XDH in WT, *atm3-1*, and *GRXS15 K83A* mutants. Equal amounts of protein
1025 (35 μ g) extracted from 8-d-old seedlings were separated on non-denaturing PA gel and stained
1026 for XDH activity using hypoxanthine as substrate.

1027 **F:** In-gel activities of aldehyde oxidase (AO) in WT and *atm3-1* as well as *grxs15* mutants. Equal
1028 amounts of protein were separated on non-denaturing PA gels and stained for AO activity using
1029 synthetic aldehydes (1-naphthaldehyde and indole-3-carboxaldehyde) as substrates. For control
1030 of protein-loading the gel was subsequently stained with Coomassie.

1031

1032

1033 **Figure 4. Respiration in complemented Arabidopsis *grxs15* mutants.**

1034 **A:** Root respiration rate of *GRXS15 K83A* line #3 (4.5-week-old) and the respective WT grown
1035 to similar size (2-week-old) after addition of the cytochrome c oxidase inhibitor KCN (4 mM)
1036 alone or together with the alternative oxidase inhibitor propylgallate (pGal; 0.2 mM) ($n = 4$;
1037 means \pm SD). The statistical analysis (two-way ANOVA with post hoc Holm-Sidak comparisons
1038 for WT vs. *grxs15* mutant) indicated a significant difference in the respiration of mitochondria
1039 from WT and *GRXS15 K83A* line #3; ***: $P \leq 0.001$.

1040 **B:** Respiratory complexes I, II, III and V separated by BN-PAGE and visualized with Coomassie
1041 staining in WT, *GRXS15 K83A* line #4 and *GRXS15^{amiR}*. Mitochondria were purified from 4-
1042 week-old plants.

1043 **C, D:** Oxygen consumption rates for purified mitochondria from WT and *GRXS15 K83A* line #3
1044 energized with succinate or pyruvate/malate. O₂ consumption was measured before (blank) and
1045 after addition of mitochondria (mito). State II respiration was initiated by the addition of the
1046 respective substrate (state II; succinate (10 mM succinate, 0.25 mM ATP) or pyruvate/malate
1047 (10 mM pyruvate, 10 mM malate, 0.3 mM NAD and 0.1 mM thiamine pyrophosphate). State III
1048 respiration was initiated by the addition of 50 μ M ADP. State IV represents the respiration after
1049 ADP consumption and CCCP shows the respiration after addition of the protonophore carbonyl
1050 cyanide *m*-chlorophenylhydrazine (CCCP; 10 μ M), which uncouples electron transport from
1051 ATP synthesis. All results are based on three independent preparations of mitochondria and are
1052 shown as means \pm SEM.

1053

1054 **Figure 5 Aconitase activities in mitochondria of *grxs15* mutants.**

1055 **A:** Aconitase activity of *GRXS15^{amiR}* and *GRXS15 K83A* line #4 compared to the respective
1056 WTs from isolated mitochondria. $n = 2$.

1057 **B:** Protein gel blot analysis probed with antiserum raised against Arabidopsis ACO. 9 μ g of
1058 protein isolated from mitochondria of a wild-type plant as well as *GRXS15^{amiR}* and *GRXS15*
1059 *K83A* lines #4 were loaded onto the gel. ACO and translocase of the mitochondria 40 (TOM40)
1060 protein levels were visualized by immunoblotting under denaturing conditions. Total protein
1061 staining served as a loading control.

1062

1063

1064 **Figure 6. Organic acids of the TCA cycle accumulate in Arabidopsis *GRXS15 K83A***
1065 **mutants.**

1066 Organic acids were analyzed in 8-d-old seedlings of WT compared to *GRXS15 K83A* lines #3
1067 and #4 ($n = 4-5$; means \pm SEM). The statistical analysis (one-way ANOVA with post hoc Holm-
1068 Sidak comparisons for WT vs. mutant lines) indicated significant changes; *: $P \leq 0.05$; ***:
1069 $P \leq 0.001$.

1070

1071

1072 **Figure 7. Lipoyl cofactor-dependent enzymes are affected in Arabidopsis *GRXS15 K83A***
1073 **mutants.**

1074 **A:** Immunoblot analysis using antibodies against glycine dehydrogenase H-protein (H1-3), lipoyl
1075 cofactor (LC) as well as antibodies against TOM40 for a loading control and *GRXS15*. 15 μ g of
1076 isolated mitochondria were loaded per lane.

1077 **B:** Pyruvate dehydrogenase complex (PDC) activity in isolated mitochondria. Reduction of
1078 NAD^+ was measured in mitochondria isolated from 14-d-old seedlings of WT and the *GRXS15*
1079 *K83A* line #3 ($n = 5$; means \pm SEM). The statistical analysis (one-way ANOVA with post hoc
1080 Holm-Sidak comparisons for WT vs. *grxs15* mutant) indicated significant changes; * $P \leq 0.05$).

1081 **C:** Relative abundance of amino acids in 8-d-old seedlings of WT compared *GRXS15 K83A*
1082 lines #3 and #4. WT was set to 100% ($n = 4-5$, means \pm SEM). Absolute values and statistical
1083 analysis are provided in Suppl. Table S1. Amino acids were categorized after their respective
1084 common precursor. 3PG = 3-phosphoglycerate, PEP = phosphoenolpyruvate.

1085 **D:** Analysis of the breakdown products of leucine, isoleucine and valine – α -ketoisocaproic acid
1086 (KIC), α -ketoisovaleric acid (KIV), α -keto- β -methylvaleric acid (KMV) – and phenylpyruvate
1087 (PhePyr) in seedlings of WT compared to *GRXS15 K83A* lines #3 and #4. WT was set to 100%
1088 ($n = 4-5$; means \pm SEM). Absolute values are provided in Suppl. Table S1. The statistical
1089 analysis (two-way ANOVA with post hoc Holm-Sidak comparisons for WT vs. *grxs15* mutant)
1090 indicated significant changes; ** $P \leq 0.01$; *** $P \leq 0.001$.

1091 **Figure 8. Lipoylation of mitochondrial proteins depends on GRXS15.**

1092 **A:** Distribution of Fe-S clusters in Arabidopsis mitochondria to soluble Fe-S proteins and
1093 lipoylation of proteins via lipoyl synthase (LIP1). Putative transfer of Fe-S clusters is indicated by
1094 solid arrows for [2Fe-2S] and dashed arrows for [4Fe-4S]. Intermediate complexes of Fe-S
1095 transfer and assembly of [4Fe-4S] clusters are not shown. mFDX1/2: mitochondrial ferredoxin
1096 1/2; ACO2/3; aconitase 2/3; BIO2: biotin synthase 2; CNX2: GTP-3',8-cyclase PDC: pyruvate
1097 decarboxylase complex; OGDC: 2-oxoglutarate dehydrogenase complex; GDC: glycine
1098 decarboxylase complex; BCKDC: branched-chain α -keto acid dehydrogenase complex; LC:
1099 Lipoyl cofactor. Numbers give the estimated copy number of the respective proteins according
1100 to Fuchs et al. (2020).

1101 **B:** Abundance of subunits in the four mitochondrial dehydrogenase complexes PDC, GDC,
1102 OGDC and BCKDC according to Fuchs et al. (2020). The copy number for the H subunit of
1103 GDC is only for the isoform H2, because the nominally more abundant isoforms H1 and H3 (see
1104 Fig. 7A) were not identified by Fuchs et al. (2020). E3 and L subunits are formed by the closely
1105 related and highly similar proteins mtLPD1 (4876 copies) and mtLPD2 (10114 copies), The total
1106 of both isoforms is given but it should be noted that a preference of GDC for mtLPD1 and of the
1107 other three complexes for mtLPD2 has been proposed (Lutziger and Oliver, 2001). Deficiencies
1108 of these enzymes generates metabolic bottlenecks and causes an increase of their respective
1109 substrates and particularly for PDC and OGDC also a severe limit in carbon supply to the TCA
1110 cycle.

1111

1112

1113

Parsed Citations

- Albrecht, S.C., Sobotta, M.C., Bausewein, D., Aller, I., Hell, R., Dick, T.P., and Meyer, A.J. (2014).** Redesign of genetically encoded biosensors for monitoring mitochondrial redox status in a broad range of model eukaryotes. *J. Biomol. Screen.* 19: 379–386.
Pubmed: [Author and Title](#)
Google Scholar: [Author Only Title Only Author and Title](#)
- Araújo, W.L., Ishizaki, K., Nunes-Nesi, A., Larson, T.R., Tohge, T., Krahnert, I., Witt, S., Obata, T., Schauer, N., Graham, I.A., Leaver, C.J., and Fernie, A.R. (2010).** Identification of the 2-hydroxyglutarate and isovaleryl-CoA dehydrogenases as alternative electron donors linking lysine catabolism to the electron transport chain of Arabidopsis mitochondria. *Plant Cell* 22: 1549–1563.
Pubmed: [Author and Title](#)
Google Scholar: [Author Only Title Only Author and Title](#)
- Baker, P.R., Friederich, M.W., Swanson, M.A., Shaikh, T., Bhattacharya, K., Scharer, G.H., Aicher, J., Creadon-Swindell, G., Geiger, E., MacLean, K.N. et al. (2014).** Variant non ketotic hyperglycinemia is caused by mutations in LIAS, BOLA3 and the novel gene GLRX5. *Brain* 137: 366–379.
Pubmed: [Author and Title](#)
Google Scholar: [Author Only Title Only Author and Title](#)
- Banci, L., Brancaccio, D., Ciofi-Baffoni, S., Del Conte, R., Gadepalli, R., Mikolajczyk, M., Neri, S., Piccioli, M., and Winkelmann, J. (2014).** [2Fe-2S] cluster transfer in iron–sulfur protein biogenesis. *Proc. Natl. Acad. Sci.* 111: 6203–6208.
Pubmed: [Author and Title](#)
Google Scholar: [Author Only Title Only Author and Title](#)
- Bandyopadhyay, S., Gama, F., Molina-Navarro, M.M., Gualberto, J.M., Claxton, R., Naik, S.G., Huynh, B.H., Herrero, E., Jacquot, J.P., Johnson, M.K., and Rouhier, N. (2008).** Chloroplast monothiol glutaredoxins as scaffold proteins for the assembly and delivery of [2Fe–2S] clusters. *EMBO J.* 27: 1122–1133.
Pubmed: [Author and Title](#)
Google Scholar: [Author Only Title Only Author and Title](#)
- Begas, P., Liedgens, L., Moseler, A., Meyer, A.J., and Deponte, M. (2017).** Glutaredoxin catalysis requires two distinct glutathione interaction sites. *Nat. Commun.* 8: 14835.
Pubmed: [Author and Title](#)
Google Scholar: [Author Only Title Only Author and Title](#)
- Belin, C., Bashandy, T., Cela, J., Delmore-Hinoux, V., Riondet, C., and Reichheld, J.P. (2015).** A comprehensive study of thiol reduction gene expression under stress conditions in Arabidopsis thaliana. *Plant. Cell Environ.* 38: 299–314.
Pubmed: [Author and Title](#)
Google Scholar: [Author Only Title Only Author and Title](#)
- Bernard, D.G., Cheng, Y., Zhao, Y., and Balk, J. (2009).** An allelic mutant series of ATM3 reveals its key role in the biogenesis of cytosolic iron-sulfur proteins in Arabidopsis. *Plant Physiol.* 151: 590–602.
Pubmed: [Author and Title](#)
Google Scholar: [Author Only Title Only Author and Title](#)
- Bittner, F. (2014).** Molybdenum metabolism in plants and crosstalk to iron. *Front. Plant Sci.* 5: 28.
Pubmed: [Author and Title](#)
Google Scholar: [Author Only Title Only Author and Title](#)
- Browse, J., McCourt, P.J., and Somerville, C.R. (1986).** Fatty acid composition of leaf lipids determined after combined digestion and fatty acid methyl ester formation from fresh tissue. *Anal. Biochem.* 152: 141–145.
Pubmed: [Author and Title](#)
Google Scholar: [Author Only Title Only Author and Title](#)
- Cao, P., Kim, S.-J., Xing, A., Schenck, C.A., Liu, L., Jiang, N., Wang, J., Last, R.L., and Brandizzi, F. (2019).** Homeostasis of branched-chain amino acids is critical for the activity of TOR signaling in Arabidopsis. *Elife* 8: e50747.
Pubmed: [Author and Title](#)
Google Scholar: [Author Only Title Only Author and Title](#)
- Carrari, F., Nunes-Nesi, A., Gibon, Y., Lytovchenko, A., Loureiro, M.E., and Fernie, A.R. (2003).** Reduced expression of aconitase results in an enhanced rate of photosynthesis and marked shifts in carbon partitioning in illuminated leaves of wild species tomato. *Plant Physiol.* 133: 1322–1335.
Pubmed: [Author and Title](#)
Google Scholar: [Author Only Title Only Author and Title](#)
- Castro, L., Tórtora, V., Mansilla, S., and Radi, R. (2019).** Aconitases: Non-redox iron–sulfur proteins sensitive to reactive species. *Acc. Chem. Res.* 52: 2609–2619.
Pubmed: [Author and Title](#)
Google Scholar: [Author Only Title Only Author and Title](#)
- Cheng, N.-H., Liu, J.-Z., Brock, A., Nelson, R.S., and Hirschi, K.D. (2006).** AtGRXcp, an Arabidopsis chloroplastic glutaredoxin, is critical for protection against protein oxidative damage. *J. Biol. Chem.* 281: 26280–26288.
Pubmed: [Author and Title](#)
Google Scholar: [Author Only Title Only Author and Title](#)

Cheng, N.-H., Liu, J.-Z., Liu, X., Wu, Q., Thompson, S.M., Lin, J., Chang, J., Whitham, S.A., Park, S., Cohen, J.D., and Hirschi, K.D. (2011). Arabidopsis monothiol glutaredoxin, AtGRXS17, is critical for temperature-dependent postembryonic growth and development via modulating auxin response. J. Biol. Chem. 286: 20398–20406.

Pubmed: [Author and Title](#)

Google Scholar: [Author Only Title Only Author and Title](#)

De Col, V. et al. (2017). ATP sensing in living plant cells reveals tissue gradients and stress dynamics of energy physiology. Elife 6: e26770.

Pubmed: [Author and Title](#)

Google Scholar: [Author Only Title Only Author and Title](#)

Couturier, J., Przybyla-Toscano, J., Roret, T., Didierjean, C., and Rouhier, N. (2015). The roles of glutaredoxins ligating Fe–S clusters: Sensing, transfer or repair functions? Biochim. Biophys. Acta - Mol. Cell Res. 1853: 1513–1527.

Pubmed: [Author and Title](#)

Google Scholar: [Author Only Title Only Author and Title](#)

Deponte, M. (2013). Glutathione catalysis and the reaction mechanisms of glutathione-dependent enzymes. Biochim. Biophys. Acta - Gen. Subj. 1830: 3217–3266.

Pubmed: [Author and Title](#)

Google Scholar: [Author Only Title Only Author and Title](#)

Douce, R., Bourguignon, J., Neuburger, M., and Rébeillé, F. (2001). The glycine decarboxylase system: a fascinating complex. Trends Plant Sci. 6: 167–176.

Pubmed: [Author and Title](#)

Google Scholar: [Author Only Title Only Author and Title](#)

Ewald, R., Hoffmann, C., Florian, A., Neuhaus, E., Fernie, A.R., and Bauwe, H. (2014). Lipoate-protein ligase and octanoyltransferase are essential for protein lipoylation in mitochondria of Arabidopsis. Plant Physiol. 165: 978–990.

Pubmed: [Author and Title](#)

Google Scholar: [Author Only Title Only Author and Title](#)

Figueroa, P., León, G., Elorza, A., Holuigue, L., and Jordana, X. (2001). Three different genes encode the iron-sulfur subunit of succinate dehydrogenase in Arabidopsis thaliana. Plant Mol. Biol. 46: 241–250.

Pubmed: [Author and Title](#)

Google Scholar: [Author Only Title Only Author and Title](#)

Fricker, M.D. (2016). Quantitative redox imaging software. Antioxid. Redox Signal. 24: 752–762.

Pubmed: [Author and Title](#)

Google Scholar: [Author Only Title Only Author and Title](#)

Fuchs, P. Rugen, N. Carrie, C. Elsässer, M. Finkemeier, I. Giese, J. Hildebrandt, T.M. Kühn, K. Maurino, V.G. Ruberti, C. et al. (2020). Single organelle function and organization as estimated from Arabidopsis mitochondrial proteomics. Plant J. 101: 420–441.

Pubmed: [Author and Title](#)

Google Scholar: [Author Only Title Only Author and Title](#)

Gu, L., Jones, A.D., and Last, R.L. (2010). Broad connections in the Arabidopsis seed metabolic network revealed by metabolite profiling of an amino acid catabolism mutant. Plant J. 61: 579–590.

Pubmed: [Author and Title](#)

Google Scholar: [Author Only Title Only Author and Title](#)

Hesberg, C., Hänsch, R., Mendel, R.R., and Bittner, F. (2004). Tandem orientation of duplicated xanthine dehydrogenase genes from Arabidopsis thaliana: Differential gene expression and enzyme activities. J. Biol. Chem. 279: 13547–13554.

Pubmed: [Author and Title](#)

Google Scholar: [Author Only Title Only Author and Title](#)

Hildebrandt, T.M., Nunes Nesi, A., Araújo, W.L., and Braun, H.-P. (2015). Amino acid catabolism in plants. Mol. Plant 8: 1563–1579.

Pubmed: [Author and Title](#)

Google Scholar: [Author Only Title Only Author and Title](#)

Hoffmann, C., Plochanski, B., Haferkamp, I., Leroch, M., Ewald, R., Bauwe, H., Riemer, J., Herrmann, J.M., and Neuhaus, H.E. (2013). From endoplasmic reticulum to mitochondria: Absence of the Arabidopsis ATP antiporter Endoplasmic Reticulum Adenylate Transporter1 perturbs photorespiration. Plant Cell 25: 2647–2660.

Pubmed: [Author and Title](#)

Google Scholar: [Author Only Title Only Author and Title](#)

Huang, S., Taylor, N.L., Ströher, E., Fenske, R., and Millar, A.H. (2013). Succinate dehydrogenase assembly factor 2 is needed for assembly and activity of mitochondrial complex II and for normal root elongation in Arabidopsis. Plant J. 73: 429–441.

Pubmed: [Author and Title](#)

Google Scholar: [Author Only Title Only Author and Title](#)

Igamberdiev, A.U., Bykova, N. V, Lea, P.J., and Gardeström, P. (2001). The role of photorespiration in redox and energy balance of photosynthetic plant cells: A study with a barley mutant deficient in glycine decarboxylase. Physiol. Plant. 111: 427–438.

Pubmed: [Author and Title](#)

Google Scholar: [Author Only Title Only Author and Title](#)

Iñigo, S. et al. (2016). Glutaredoxin GRXS17 associates with the cytosolic iron-sulfur cluster assembly pathway. *Plant Physiol.* 172: 858–873.

Pubmed: [Author and Title](#)

Google Scholar: [Author Only Title Only Author and Title](#)

Ishizaki, K., Larson, T.R., Schauer, N., Fernie, A.R., Graham, I.A., and Leaver, C.J. (2005). The critical role of Arabidopsis electron-transfer flavoprotein:ubiquinone oxidoreductase during dark-induced starvation. *Plant Cell* 17: 2587–2600.

Pubmed: [Author and Title](#)

Google Scholar: [Author Only Title Only Author and Title](#)

Knesting, J. et al. (2015). Arabidopsis glutaredoxin S17 and its partner, the nuclear factor Y subunit C11/negative cofactor 2 α , contribute to maintenance of the shoot apical meristem under long-day photoperiod. *Plant Physiol.* 167: 1643–1658.

Pubmed: [Author and Title](#)

Google Scholar: [Author Only Title Only Author and Title](#)

Koshiba, T., Saito, E., Ono, N., Yamamoto, N., and Sato, M. (1996). Purification and properties of flavin- and molybdenum-containing aldehyde oxidase from coleoptiles of maize. *Plant Physiol.* 110: 781–789.

Pubmed: [Author and Title](#)

Google Scholar: [Author Only Title Only Author and Title](#)

Kruse, I., Maclean, A.E., Hill, L., and Balk, J. (2018). Genetic dissection of cyclic pyranopterin monophosphate biosynthesis in plant mitochondria. *Biochem. J.* 475: 495–509.

Pubmed: [Author and Title](#)

Google Scholar: [Author Only Title Only Author and Title](#)

Kühn, K., Obata, T., Feher, K., Bock, R., Fernie, A.R., and Meyer, E.H. (2015). Complete mitochondrial complex I deficiency induces an up-regulation of respiratory fluxes that is abolished by traces of functional complex I. *Plant Physiol.* 168: 1537–1549.

Pubmed: [Author and Title](#)

Google Scholar: [Author Only Title Only Author and Title](#)

Lill, R. and Freibert, S.-A. (2020). Mechanisms of mitochondrial iron-sulfur protein biogenesis. *Annu. Rev. Biochem.* 89: 1.

Pubmed: [Author and Title](#)

Google Scholar: [Author Only Title Only Author and Title](#)

Lillig, C.H., Berndt, C., and Holmgren, A. (2008). Glutaredoxin systems. *Biochim. Biophys. Acta - Gen. Subj.* 1780: 1304–1317.

Pubmed: [Author and Title](#)

Google Scholar: [Author Only Title Only Author and Title](#)

Liu, G., Wang, Y., Anderson, G.J., Camaschella, C., Chang, Y., and Nie, G. (2016). Functional analysis of GLRX5 mutants reveals distinct functionalities of GLRX5 protein. *J. Cell. Biochem.* 117: 207–217.

Pubmed: [Author and Title](#)

Google Scholar: [Author Only Title Only Author and Title](#)

Lutziger, I. and Oliver, D.J. (2001). Characterization of two cDNAs encoding mitochondrial lipoamide dehydrogenase from Arabidopsis. *Plant Physiol.* 127: 615–623.

Pubmed: [Author and Title](#)

Google Scholar: [Author Only Title Only Author and Title](#)

McCarthy, E.L. and Booker, S.J. (2017). Destruction and reformation of an iron-sulfur cluster during catalysis by lipoyl synthase. *Science.* 358: 373–377.

Pubmed: [Author and Title](#)

Google Scholar: [Author Only Title Only Author and Title](#)

Meinke, D.W. (2019). Genome-wide identification of EMBRYO-DEFECTIVE (EMB) genes required for growth and development in Arabidopsis. *New Phytol.*: 1–20.

Pubmed: [Author and Title](#)

Google Scholar: [Author Only Title Only Author and Title](#)

Meyer, A.J. and Fricker, M.D. (2000). Direct measurement of glutathione in epidermal cells of intact Arabidopsis roots by two-photon laser scanning microscopy. *J. Microsc.* 198: 174–181.

Pubmed: [Author and Title](#)

Google Scholar: [Author Only Title Only Author and Title](#)

Meyer, E.H., Solheim, C., Tanz, S.K., Bonnard, G., and Millar, A.H. (2011). Insights into the composition and assembly of the membrane arm of plant complex I through analysis of subcomplexes in Arabidopsis mutant lines. *J. Biol. Chem.* 286: 26081–26092.

Pubmed: [Author and Title](#)

Google Scholar: [Author Only Title Only Author and Title](#)

Meyer, E.H., Welchen, E., and Carrie, C. (2019). Assembly of the complexes of the oxidative phosphorylation system in land plant mitochondria. *Annu. Rev. Plant Biol.* 70: 23–50.

Pubmed: [Author and Title](#)

Google Scholar: [Author Only Title Only Author and Title](#)

Meyer, Y., Buchanan, B.B., Vignols, F., and Reichheld, J.-P. (2009). Thioredoxins and glutaredoxins: Unifying elements in redox biology.

Annu. Rev. Genet. 43: 335–367.

Pubmed: [Author and Title](#)

Google Scholar: [Author Only Title Only Author and Title](#)

Morgan, M.J., Lehmann, M., Schwarzländer, M., Baxter, C.J., Sienkiewicz-Porzucek, A., Williams, T.C.R., Schauer, N., Fernie, A.R., Fricker, M.D., Ratcliffe, R.G., Sweetlove, L.J., and Finkemeier, I. (2008). Decrease in manganese superoxide dismutase leads to reduced root growth and affects tricarboxylic acid cycle flux and mitochondrial redox homeostasis. *Plant Physiol.* 147: 101–114.

Pubmed: [Author and Title](#)

Google Scholar: [Author Only Title Only Author and Title](#)

Moseler, A., Aller, I., Wagner, S., Nietzel, T., Przybyla-Toscano, J., Mühlhoff, U., Lill, R., Berndt, C., Rouhier, N., Schwarzländer, M., and Meyer, A.J. (2015). The mitochondrial monothiol glutaredoxin S15 is essential for iron-sulfur protein maturation in *Arabidopsis thaliana*. *Proc. Natl. Acad. Sci. U. S. A.* 112: 13735–13740.

Pubmed: [Author and Title](#)

Google Scholar: [Author Only Title Only Author and Title](#)

Mouillon, J.-M., Aubert, S., Bourguignon, J., Gout, E., Douce, R., and Rébeillé, F. (1999). Glycine and serine catabolism in non-photosynthetic higher plant cells: their role in C1 metabolism. *Plant J.* 20: 197–205.

Pubmed: [Author and Title](#)

Google Scholar: [Author Only Title Only Author and Title](#)

Navarre, D.A., Wendehenne, D., Durner, J., Noad, R., and Klessig, D.F. (2000). Nitric oxide modulates the activity of tobacco aconitase. *Plant Physiol.* 122: 573–582.

Pubmed: [Author and Title](#)

Google Scholar: [Author Only Title Only Author and Title](#)

Nietzel, T., Mostertz, J., Ruberti, C., Wagner, S., Moseler, A., Fuchs, P., Müller-Schüssele, S.J., Benamar, A., Poschet, G., Büttner, M. et al. (2020). Redox-mediated kick-start of mitochondrial energy metabolism drives resource-efficient seed germination. *Proc. Natl. Acad. Sci.* 117: 741–751.

Pubmed: [Author and Title](#)

Google Scholar: [Author Only Title Only Author and Title](#)

Nietzel, T., Elsässer, M., Ruberti, C., Steinbeck, J., Ugalde, J.M., Fuchs, P., Wagner, S., Ostermann, L., Moseler, A., Lenke, P. et al (2019). The fluorescent protein sensor roGFP2-Orp1 monitors in vivo H₂O₂ and thiol redox integration and elucidates intracellular H₂O₂ dynamics during elicitor-induced oxidative burst in *Arabidopsis*. *New Phytol.* 221: 1649–1664.

Pubmed: [Author and Title](#)

Google Scholar: [Author Only Title Only Author and Title](#)

Pain, D. and Dancis, A. (2016). Roles of Fe–S proteins: from cofactor synthesis to iron homeostasis to protein synthesis. *Curr. Opin. Genet. Dev.* 38: 45–51.

Pubmed: [Author and Title](#)

Google Scholar: [Author Only Title Only Author and Title](#)

Patton, D.A., Schetter, A.L., Franzmann, L.H., Nelson, K., Ward, E.R., and Meinke, D.W. (1998). An embryo-defective mutant of *Arabidopsis* disrupted in the final step of biotin synthesis. *Plant Physiol.* 116: 935–946.

Pubmed: [Author and Title](#)

Google Scholar: [Author Only Title Only Author and Title](#)

Peng, C., Uygun, S., Shiu, S.-H., and Last, R.L. (2015). The impact of the branched-chain ketoacid dehydrogenase complex on amino acid homeostasis in *Arabidopsis*. *Plant Physiol.* 169: 1807–1820.

Pubmed: [Author and Title](#)

Google Scholar: [Author Only Title Only Author and Title](#)

Pires, M. V., Pereira Júnior, A.A., Medeiros, D.B., Daloso, D.M., Pham, P.A., Barros, K.A., Engqvist, M.K.M., Florian, A., Krahnert, I., Maurino, V.G., Araújo, W.L., and Fernie, A.R. (2016). The influence of alternative pathways of respiration that utilize branched-chain amino acids following water shortage in *Arabidopsis*. *Plant. Cell Environ.* 39: 1304–1319.

Pubmed: [Author and Title](#)

Google Scholar: [Author Only Title Only Author and Title](#)

Pommerrenig, B., Popko, J., Heilmann, M., Schulmeister, S., Dietel, K., Schmitt, B., Stadler, R., Feussner, I., and Sauer, N. (2013). SUCROSE TRANSPORTER 5 supplies *Arabidopsis* embryos with biotin and affects triacylglycerol accumulation. *Plant J.* 73: 392–404.

Pubmed: [Author and Title](#)

Google Scholar: [Author Only Title Only Author and Title](#)

Rey, P., Becuwe, N., Tourrette, S., and Rouhier, N. (2017). Involvement of *Arabidopsis* glutaredoxin S14 in the maintenance of chlorophyll content. *Plant. Cell Environ.* 40: 2319–2332.

Pubmed: [Author and Title](#)

Google Scholar: [Author Only Title Only Author and Title](#)

Rodríguez-Manzanares, M.T., Ros, J., Cabisco, E., Sorribas, A., and Herrero, E. (1999). Grx5 glutaredoxin plays a central role in protection against protein oxidative damage in *Saccharomyces cerevisiae*. *Mol. Cell. Biol.* 19: 8180–8190.

Pubmed: [Author and Title](#)

Google Scholar: [Author Only Title Only Author and Title](#)

Rodríguez-Manzanares, M.T., Tamarit, J., Belli, G., Ros, J., and Herrero, E. (2002). Grx5 is a mitochondrial glutaredoxin required for the activity of iron/sulfur enzymes. *Mol. Biol. Cell* 13: 1109–1121.

Pubmed: [Author and Title](#)

Google Scholar: [Author Only Title Only Author and Title](#)

Rouhier, N., Lemaire, S.D., and Jacquot, J.-P. (2008). The role of glutathione in photosynthetic organisms: Emerging functions for glutaredoxins and glutathionylation. *Annu. Rev. Plant Biol.* 59: 143–166.

Pubmed: [Author and Title](#)

Google Scholar: [Author Only Title Only Author and Title](#)

Sarasketa, A, González-Moro, M.B., González-Murua, C., and Marino, D. (2014). Exploring ammonium tolerance in a large panel of *Arabidopsis thaliana* natural accessions. *J. Exp. Bot.* 65: 6023–6033.

Pubmed: [Author and Title](#)

Google Scholar: [Author Only Title Only Author and Title](#)

Schaedler, T.A., Thornton, J.D., Kruse, I., Schwarzländer, M., Meyer, A.J., van Veen, H.W., and Balk, J. (2014). A conserved mitochondrial ATP-binding cassette transporter exports glutathione polysulfide for cytosolic metal cofactor assembly. *J. Biol. Chem.* 289: 23264–23274.

Pubmed: [Author and Title](#)

Google Scholar: [Author Only Title Only Author and Title](#)

Scheible, W.-R., Lauerer, M., Schulze, E.-D., Caboche, M., and Stitt, M. (1997). Accumulation of nitrate in the shoot acts as a signal to regulate shoot-root allocation in tobacco. *Plant J.* 11: 671–691.

Pubmed: [Author and Title](#)

Google Scholar: [Author Only Title Only Author and Title](#)

Schneider, T., Dinkins, R., Robinson, K., Shellhammer, J., and Meinke, D.W. (1989). An embryo-lethal mutant of *Arabidopsis thaliana* is a biotin auxotroph. *Dev. Biol.* 131: 161–167.

Pubmed: [Author and Title](#)

Google Scholar: [Author Only Title Only Author and Title](#)

Schwarz, G. and Mendel, R.R. (2006). Molybdenum cofactor biosynthesis and molybdenum enzymes. *Annu. Rev. Plant Biol.* 57: 623–647.

Pubmed: [Author and Title](#)

Google Scholar: [Author Only Title Only Author and Title](#)

Senkler, J., Senkler, M., Eubel, H., Hildebrandt, T., Lengwenus, C., Schertl, P., Schwarzländer, M., Wagner, S., Wittig, I., and Braun, H.-P. (2017). The mitochondrial complexome of *Arabidopsis thaliana*. *Plant J.* 89: 1079–1092.

Pubmed: [Author and Title](#)

Google Scholar: [Author Only Title Only Author and Title](#)

Solbiati, J., Chapman-Smith, A., and Cronan, J.E. (2002). Stabilization of the biotinoyl domain of *Escherichia coli* acetyl-CoA carboxylase by interactions between the attached biotin and the protruding "thumb" structure. *J. Biol. Chem.* 277: 21604–21609.

Pubmed: [Author and Title](#)

Google Scholar: [Author Only Title Only Author and Title](#)

Solomonson, A. and DeBerardinis, R.J. (2018). Lipoic acid metabolism and mitochondrial redox regulation. *J. Biol. Chem.* 293: 7522–7530.

Pubmed: [Author and Title](#)

Google Scholar: [Author Only Title Only Author and Title](#)

Ströher, E., Grassl, J., Carrie, C., Fenske, R., Whelan, J., and Millar, A.H. (2016). Glutaredoxin S15 is involved in Fe-S cluster transfer in mitochondria influencing lipoic acid-dependent enzymes, plant growth, and arsenic tolerance in *Arabidopsis*. *Plant Physiol.* 170: 1284–1299.

Pubmed: [Author and Title](#)

Google Scholar: [Author Only Title Only Author and Title](#)

Sweetlove, L.J., Taylor, N.L., and Leaver, C.J. (2007). Isolation of intact, functional mitochondria from the model plant *Arabidopsis thaliana*. In *Mitochondria: Practical Protocols*, D. Leister and J.M. Herrmann, eds (Humana Press: Totowa, NJ), pp. 125–136.

Pubmed: [Author and Title](#)

Google Scholar: [Author Only Title Only Author and Title](#)

Taylor, N.L., Heazlewood, J.L., Day, D.A., and Millar, A.H. (2004). Lipoic acid-dependent oxidative catabolism of α -keto acids in mitochondria provides evidence for branched-chain amino acid catabolism in *Arabidopsis*. *Plant Physiol.* 134: 838–848.

Pubmed: [Author and Title](#)

Google Scholar: [Author Only Title Only Author and Title](#)

Teschner, J., Lachmann, N., Schulze, J., Geisler, M., Selbach, K., Santamaria-Araujo, J., Balk, J., Mendel, R.R., and Bittner, F. (2010). A novel role for *Arabidopsis* mitochondrial ABC transporter ATM3 in molybdenum cofactor biosynthesis. *Plant Cell* 22: 468–480.

Pubmed: [Author and Title](#)

Google Scholar: [Author Only Title Only Author and Title](#)

Thordal-Christensen, H., Zhang, Z., Wei, Y., and Collinge, D.B. (1997). Subcellular localization of H₂O₂ in plants. H₂O₂ accumulation in papillae and hypersensitive response during the barley-powdery mildew interaction. *Plant J.* 11: 1187–1194.

Pubmed: [Author and Title](#)

Google Scholar: [Author Only Title Only Author and Title](#)

Ugulava, N.B., Sacanell, C.J., and Jarrett, J.T. (2001). Spectroscopic changes during a single turnover of biotin synthase: destruction of a [2Fe-2S] cluster accompanies sulfur insertion. *Biochemistry* 40: 8352–8358.

Pubmed: [Author and Title](#)

Google Scholar: [Author Only](#) [Title Only](#) [Author and Title](#)

Uzarska, M.A., Dutkiewicz, R., Freibert, S.-A., Lill, R., and Mühlenhoff, U. (2013). The mitochondrial Hsp70 chaperone Ssq1 facilitates Fe/S cluster transfer from Isu1 to Grx5 by complex formation. *Mol. Biol. Cell* 24: 1830–1841.

Pubmed: [Author and Title](#)

Google Scholar: [Author Only](#) [Title Only](#) [Author and Title](#)

Verniquet, F., Gaillard, J., Neuburger, M., and Douce, R. (1991). Rapid inactivation of plant aconitase by hydrogen peroxide. *Biochem. J.* 276: 643–648.

Pubmed: [Author and Title](#)

Google Scholar: [Author Only](#) [Title Only](#) [Author and Title](#)

Voon, C.P., Guan, X., Sun, Y., Sahu, A., Chan, M.N., Gardeström, P., Wagner, S., Fuchs, P., Nietzel, T., Versaw, W.K., Schwarzländer, M., and Lim, B.L. (2018). ATP compartmentation in plastids and cytosol of *Arabidopsis thaliana* revealed by fluorescent protein sensing. *Proc. Natl. Acad. Sci.* 115: 10778–10787.

Pubmed: [Author and Title](#)

Google Scholar: [Author Only](#) [Title Only](#) [Author and Title](#)

Wagner, S., Behera, S., De Bortoli, S., Logan, DC., Fuchs, P., Carraretto, L., Teardo, E., Cendron, L., Nietzel, T., Füßl, M., et al. (2015). The EF-hand Ca²⁺ binding protein MICU choreographs mitochondrial Ca²⁺ dynamics in *Arabidopsis*. *Plant Cell* 27: 3190–3212.

Pubmed: [Author and Title](#)

Google Scholar: [Author Only](#) [Title Only](#) [Author and Title](#)

Wang, R., Tischner, R., Gutiérrez, R.A., Hoffman, M., Xing, X., Chen, M., Coruzzi, G., and Crawford, N.M. (2004). Genomic analysis of the nitrate response using a nitrate reductase-null mutant of *Arabidopsis*. *Plant Physiol.* 136: 2512–2522.

Pubmed: [Author and Title](#)

Google Scholar: [Author Only](#) [Title Only](#) [Author and Title](#)

Wilkinson, J.Q. and Crawford, N.M. (1993). Identification and characterization of a chlorate-resistant mutant of *Arabidopsis thaliana* with mutations in both nitrate reductase structural genes NIA1 and NIA2. *Mol. Gen. Genet.* 239: 289–297.

Pubmed: [Author and Title](#)

Google Scholar: [Author Only](#) [Title Only](#) [Author and Title](#)

Yang, Y., M. Pollard, A., Höfler, C., Poschet, G., Wirtz, M., Hell, R., and Sourjik, V. (2015). Relation between chemotaxis and consumption of amino acids in bacteria. *Mol. Microbiol.* 96: 1272–1282.

Pubmed: [Author and Title](#)

Google Scholar: [Author Only](#) [Title Only](#) [Author and Title](#)

Yasuno, R. and Wada, H. (2002). The biosynthetic pathway for lipoic acid is present in plastids and mitochondria in *Arabidopsis thaliana*. *FEBS Lett.* 517: 110–114.

Pubmed: [Author and Title](#)

Google Scholar: [Author Only](#) [Title Only](#) [Author and Title](#)

Ye, H., Jeong, S.Y., Ghosh, M.C., Kovtunovych, G., Silvestri, L., Ortillo, D., Uchida, N., Tisdale, J., Camaschella, C., and Rouault, T.A. (2010). Glutaredoxin 5 deficiency causes sideroblastic anemia by specifically impairing heme biosynthesis and depleting cytosolic iron in human erythroblasts. *J. Clin. Invest.* 120: 1749–1761.

Pubmed: [Author and Title](#)

Google Scholar: [Author Only](#) [Title Only](#) [Author and Title](#)

Yu, H., Du, X., Zhang, F., Zhang, F., Hu, Y., Liu, S., Jiang, X., Wang, G., and Liu, D. (2012). A mutation in the E2 subunit of the mitochondrial pyruvate dehydrogenase complex in *Arabidopsis* reduces plant organ size and enhances the accumulation of amino acids and intermediate products of the TCA Cycle. *Planta* 236: 387–399.

Pubmed: [Author and Title](#)

Google Scholar: [Author Only](#) [Title Only](#) [Author and Title](#)

Zhang, Y., Swart, C., Aseekh, S., Scossa, F., Jiang, L., Obata, T., Graf, A., and Fernie, A.R. (2018). The extra-pathway interactome of the TCA cycle: expected and unexpected metabolic interactions. *Plant Physiol.* 177: 966–979.

Pubmed: [Author and Title](#)

Google Scholar: [Author Only](#) [Title Only](#) [Author and Title](#)